A Study of the Speed of Sound in Pure Gases and Binary Gas Mixtures

Submitted in partial fulfillment of the requirements for
the Honors College Interdisciplinary Minor and
Departmental Honors in Physics and Astronomy.

Author:

Ashley Jean Hicks

Date:

August 7th, 2013

University of Central Arkansas

Conway, AR

Reader Approval and Signatures

_____

William Slaton, Ph. D., Advisor

_____

Stephen Addison, Ph. D., 2nd Reader, Dean of CNSM

_____

Rick Scott, Ph. D., Dean of Honors College

Table of Contents

Introduction

What is sound? In its simplest definition, sound is a wave composed of oscillating areas of pressure transmitted through a medium. The speed of sound is, as the name suggests, the speed at which the sound wave will propagate through a material. The speed of sound is a characteristic property of the material in question, and in a gas it is related to the molecular weight of the gas as well as the ratio of specific heats, γ, of the gas in question.

What benefit do we gain knowing a material's sound speed? Because speed of sound is a material property, it's theoretically possible to identify a medium by experimentally measuring its speed of sound. However, the speed of sound in a medium is not necessarily unique. Experimentally determining the speed of sound in a simple, efficient manner would allow for a narrowing down of the possibilities of what an unknown material is.

A simple, efficient, and accurate method of measuring the sound speed through a medium could have many uses. As an undergraduate lab, the experiment serves as a check of concepts on waves and sound that were developed in Modern Physics. On the right scale, the detector could be used as a detector of harmful gases in an environment. As an exploratory tool, the experiment could possibly be used to probe previously un-researched gases and gas mixtures.

One way to identify the speed of sound in a medium is to first determine the ratio of specific heats, γ. The ratio of specific heats can be determined by looking at how a sound attenuates, or loses energy, through the medium. While this method is elegant, we decide to pursue a more fundamental method of measuring the speed of sound—identifying the frequencies at which the system in question (say a pipe filled with a gas) resonates.

The Wave Equation and Resonance Frequencies in the System

To determine the resonance frequencies of a system, we must first look at the linear wave equation found from a combination of the equation of continuity, the equation of state, and Euler's equation[1]:

$$\nabla^2 P = \frac{1}{c^2}\frac{\partial^2 P}{\partial t^2} \tag{1}$$

For a cylindrical geometry the wave equation can be written in cylindrical coordinates.

$$\frac{\partial^2 P}{\partial r} + \frac{1}{r}\frac{\partial P}{\partial r} + \frac{1}{r^2}\frac{\partial^2 P}{\partial \theta^2} + \frac{\partial^2 P}{\partial z^2} + k^2 P = 0 \tag{2}$$

We know that there can be no gas flowing through the walls of our cylinder. This implies that the velocity at the wall of the cylinder is zero. Velocity can be defined as a derivative of the function, *P*, so we develop the following boundary conditions for the system that is closed at ends with rigid walls, a length *L*, and a radius *a*,:

$$\left(\frac{\partial P}{\partial z}\right)_{z=0} = \left(\frac{\partial P}{\partial z}\right)_{z=L} = \left(\frac{\partial P}{\partial r}\right)_{r=a} = 0 \tag{3}$$

To determine an exact solution for equation 2, we assume that the solution will be of the form

$$P(r, \theta, z) = R(r)\Theta(\theta)Z(z) \tag{4}$$

Separation of variables using this assumed solution yields three total differential equations

$$\frac{d^2 Z}{dz^2} = -k_{zl}^2 Z \tag{5}$$

$$\frac{d^2 \Theta}{d\theta^2} = -m^2 \Theta \tag{6}$$

$$r^2\frac{d^2R}{dr^2} + r\frac{dR}{dr} + (k_{mn}^2 r^2 - m^2)R = 0 \tag{7}$$

These equations have the following solutions[2]:

$$\mathrm{Z} = \cos k_{zl} z \tag{8}$$

$$\Theta = \cos(m\theta + \phi_{lmn}) \tag{9}$$

$$R = J_m(k_{mn} r) \tag{10}$$

where J_m is the mth Bessel function of the first kind. To determine longitudinal resonance frequencies, we look at Eq. 8. This form should look familiar from materials covered in introductory physics. To determine the frequencies where this function is a maximum for the length of the pipe, L, we take the derivative and set it equal to zero.

$$0 = -k_{zl}\sin(k_{zl}L) \tag{11}$$

A wave number, k, of zero would obviously satisfy the equation, but it isn't interesting! We look instead for values which will make the sine term zero or:

$$k_{zl}L = n\pi, n = 1, 2, 3 \ldots \tag{12}$$

Using the standard definition of wave number we can obtain an equation in terms of frequency, f, nodal number, n, and speed of sound in the medium, c.

$$\frac{2\pi f}{c}L = n\pi, n = 1, 2, 3 \ldots \tag{13}$$

With a little rearranging, we can turn equation 13 into an equation explaining the relationship between frequency and nodal number.

$$f = \frac{c}{2L}n, n = 1, 2, 3 \ldots \tag{14}$$

If we wanted to determine the speed of sound in a medium, all we would need to do is measure a number of resonance frequencies and plot them against their nodal number, *n*. The slope of this line contains the speed of sound. In fact, the simple relationship in Eq. 14 is the basis for a majority of our experimental data collection and data analysis. There are a few other things going on in the system that are worth noting, however.

To determine the radial resonance frequencies, we look more closely at equation 10. We want the solution to *R* to be an extremum, and so we are looking for values of $k_{mn}r$ which produce extremum at the radius, *a*, of the cylindrical cavity. In other words:

$$j'_{mn} = k_{mn}a \tag{15}$$

where j'_{mn} is the *n*th extremum of the *m*th Bessel function of the first kind. In our case, we are looking at situations where *m* is 0. Kinsler and Frey present a small tabulated set of values for Bessel function extrema[3], but in order to obtain values for *n* greater than five, a tabulated set of values for the zeroes of the *m*=1 Bessel function of the first kind is used with the understanding that the zeroes for this Bessel function represent the extremum of the *m*=0 Bessel function of the first kind.[4]

If we know what value j'_{mn} should take, we can solve Eq. 15 for k_{mn}.

$$k_{mn} = \frac{j'_{mn}}{a} \tag{16}$$

From the solution, we have the definition that

$$k^2 = k_{mn}^2 + k_{zl}^2 \tag{17}$$

Recalling the relationship between wave number and frequency, we can write:

$$\left(\frac{2\pi f}{c}\right)^2 = k_{mn}^2 + k_{zl}^2 \tag{18}$$

We can now input Eqs. 12 and 16 into Eq. 18, and solve for frequency to find:

$$f = \frac{c}{2\pi}\sqrt{\left(\frac{j'_{mn}}{a}\right)^2 + \left(\frac{l\pi}{L}\right)^2} \tag{19}$$

Equation 19 is an ideal equation to use if we are looking for resonance frequencies that occur due to a combination of linear and radial effects in the cylindrical cavity. In this case, however, we are looking for purely radial resonance frequencies or cases where *l* is equal to zero. The radial resonance frequencies are then:

$$f = \frac{c}{2\pi}\left(\frac{j'_{mn}}{a}\right) \tag{20}$$

A similar argument could be made that when looking for purely longitudinal resonance frequencies we are looking for frequencies where *n* is equal to zero. In this case, Eq. 19 becomes:

$$f = \frac{c}{2\pi} l, l = 1,2,3 \ldots \tag{21}$$

where *l* is the same as the integer value *n* we defined above. This is exactly the same as Eq. 14, as we would expect.

Transducer Design and Manufacture

The capacitor transducer used in this experiment was designed and built at UCA using the designs of Sessler and West as modified by Shields and Bass [5] as a guide. The transducer is 4" in diameter. It is constructed to allow for the tensioning of a flexible metal coated plastic over a metal backing plate. When assembled, the transducer creates a parallel plate capacitor, with the brass backing plate being the bottom side, and the aluminum on top of the sheeting acting as the top plate.

The transducer uses a Delrin plastic base, with a brass backing plate and brass tensioning ring, as shown in Fig. 1. The Delrin and brass pieces were turned to the correct diameter on a lathe. The base has an outer diameter of 4" and an inner diameter of 3 ½". The brass tensioning ring has a thickness of ⅛", and inner diameter of 3 ½", and an outer diameter of 4". The backing plate has a diameter slightly smaller than the Delrin base, and rests inside of a relief cut into the base that has a depth of approximately one tenth of an inch. The total height of the backing plate is three sixteenths of an inch.

Holes for the bolts were drilled at the desired location by using the positioning system on an end mill. The backing plate is secured to the Delrin base via three 2/56 x 1 ½ inch bolts in an equilateral triangle pattern. The tensioning ring is secured to the base via 12 of the same bolts. A bolt is placed at 30° intervals around the ring, as shown in Fig. 2. A ½" hole is drilled into the back of the transducer and tapped with a ½ - 20 tap. This hole is about ½" deep and allows for the attachment of a metal positioning rod to the transducer face. The rod is used to position the transducer inside of the sound tube.

All pieces are cleaned and smoothed so there are no burrs in the metal or plastic. Brass pieces are cleaned with brass polish to give them a nice shine. The completely manufactured transducer is shown disassembled in Fig. 3. The assembled transducer can be seen in Fig. 4.

The transducer was constructed with two different thicknesses of aluminum coated polymer. The first plastic was moisture-resistant, aluminum coated polyester with a thickness of 0.002" purchased from McMaster-Carr. The film was rigid and difficult to tension properly under the brass ring. A second film was more successful. This film was a portion of a Mylar emergency blanket commonly found in first aid kits. Emergency blankets have a thickness of approximately 0.0004" and a mass of approximately 1.728×10^{-3} g/cm^3. Emergency blankets are extremely flexible. Tensioning them over the brass backing plate allows for a smooth, mirror like finish. A smooth, well tensioned top plate produces a cleaner, well defined signal.

To achieve a film that is well tensioned across the backing plate, the film is first affixed with superglue or epoxy to a heavy scrap steel ring that has a diameter larger than 5" and a mass of 939.9 grams. Care is taken to affix the scrap metal ring to the plastic side of the aluminized Mylar, in other words the aluminum side is kept facing outwards so it will not touch the brass backing plate on the transducer. Once the glue on the Mylar has dried, the ring is balanced over the transducer. In this position, the effect of gravity on the ring pulls the Mylar film snugly across the backing plate. With the heavy ring still balanced, the places in the film where a bolt should be inserted are perforated, and bolts are run through the tensioning ring, into the Delrin base, secured with a nut, and the excess Mylar is cut away.

Circuit for Amplification of Transducer Output

The transducer was found to produce a quiet sound when connected to a simple signal generator. To increase the amplitude and quality of the signal from the generator, a constant polarization is placed across the plates. Following an example in an undergraduate acoustics textbook[6], an external circuit for the transducer was constructed. The circuit allows for an application of a polarization voltage, and also acts as a low-pass filter for the signal. A schematic of the circuit used for this transducer is shown in Fig. 5.

Symbols on the circuit schematic are defined as follows: V is the sinusoidal voltage on the transducer from the signal generator. V_0 is the polarization voltage supplied via a high voltage DC power supply. C_B is a capacitor which prevents DC voltage from flowing to the power amplifier and causing a failure in the circuit. C_A and R_B act as a filter to reduce the "wiggle" on the signal from the AC components of the power supply and pass only the DC components. R_A is a 22 Ω load resistor for the transducer. Finally, C_0 is the transducer.

The value for the capacitance of our transducer is measured with a standard capacitance meter to be roughly 2 nF. The value for resistor R_A is independent of transducer capacitance, and thus is set at 22 Ω. Values for R_B, C_B and C_A are dependent on the capacitance of the transducer. The value for C_B should be much greater than C_0, and the value for R_B should be much greater than the inverse of ωC_B. When circuit elements are chosen so that they meet the above requirements, it can be safely said that they do not alter the behavior of the transducer. In our case, we have chosen to use R_B = 1 MΩ and $C_B = C_A$ = 1 μF.

All circuit components were purchased from Mouser Electronics. The circuit was first assembled on a breadboard and tested to ensure that the wiring worked to increase the signal. Once we were satisfied with the circuit, it was soldered onto a circuit board and placed into a box which allowed for easy connection to the necessary electronics. A schematic of the circuit box and its connections is shown in Fig. 6.

Characterization of the Transducer

Once the transducer was assembled and wired, we conducted several tests to characterize the transducer and its output. For these tests, a previously constructed Knowles FG-3629 microphone was used, along with a previously constructed power supply and amplifier circuit. A diagram of the power supply and amplifier circuit for the microphone can be seen in Fig. 7.

As described above, the circuit for the transducer allows for application of a constant DC polarization voltage across the plates. To determine the optimal polarization voltage, we measured the output of the transducer as we varied the voltage from the power supply.

The test is conducted with the transducer sitting on a countertop and the microphone suspended on axis above the transducer plates by a ring stand and clamp. Foam is placed around the ring stand and clamp bars to limit reflections and noise in the signal. For this test, the frequency was held at a constant 20 kHz and the distance from the transducer was fixed at approximately 20 cm.

Polarization voltage began at 0 V and increased to 300 V in 10 V increments. Microphone output voltage is read on a standard oscilloscope in mV peak to peak[7]. A graph of the results can be seen in Fig. 8. From this figure it is clear that the amplitude of signal increases linearly with the polarization voltage applied. It can be assumed that if we were to increase polarization voltage above 300 V, we would obtain higher signal strength.

However, a higher polarization voltage was not used in this setup. The power supply used in this setup is capable of reaching up to 317 V. It is possible to hook two power supplies

together to achieve a maximum voltage of 600 V, however the capacitors used in the voltage adder circuit described above are rated to withstand a maximum of 450 V. It was determined that the added signal produced by a second power supply was not necessary. As a result, 300 V was chosen to be the optimal voltage for transducer operation.

We also tested the optimal frequency range of the transducer/microphone combination by observing the shape of the received wave at varying frequencies. Again, this test was conducted on the countertop with the microphone on axis with the center of the transducer plate. Frequency range ran from 5 kHz to 220 kHz in 5 kHz steps. The signal sent from the signal generator was a standard sine wave.

It was observed that the signal received by the microphone maintained its sine characteristics until the frequency of the signal reached 145 kHz. At this point, the sine waves began to deform and take on a steeper slope on the left edge of the sine wave. At approximately 180 kHz, the waves' deformation was enough to make the received signal look like a triangular wave rather than a sine wave.

The frequency response for the Knowles FG-3629 microphone is only reported up to 10 kHz.[8] As such we are unable to say definitively if the deformation in the wave is caused by a failing in the transducer or a failing in the microphone element. Either way, it was decided that the optimal performance of the transducer was between 1 kHz and 100 kHz, where the received wave maintained its sine characteristics.

As a test of the transducer's capability, we attempted to recreate near-field pressure amplitude patterns as described in Kinsler and Frey's *Fundamentals of Acoustics*[9]. Again, this test was conducted on the countertop with the microphone on axis with the center of

the transducer plate. However, instead of the microphone being held a stationary distance away, it is attached to a pair of calipers that allows for the microphone to be moved in small steps upward from the center of the transducer. Measurements of peak to peak voltage amplitude are taken every half millimeter from 1 mm to 50 mm from the transducer face. After 50 mm, measurements are taken every 1 mm up to the limits of the reach of the caliper at approximately 134.5 mm.

A graph of the resultant data is presented in Fig. 9. It is obvious from the figure that something is keeping our experimental measurements from matching with the theoretical values calculated from Kinsler and Frey's explanation. Data matches closely during the first 10 mm of data collection, but after that the experimental data presents an oscillating pattern not present in the theory. We believe that we are experiencing interference from reflections of the sound wave that skews our data. As stated above, the experiment is conducted on a countertop and while care is taken to minimize the reflections from the microphone stand, there is still a possibility of reflections from the counter, shelving above the counter, the caliper base, or other objects in the vicinity of the experiment.

To more accurately test the near-field pressure amplitude patterns of our transducer, it would be necessary to build an acoustically isolated box in which to make the measurements. In the interest of time, and because the data was not necessary to optimize the transducer for use in the experimental setup, this work was left to a future student to pursue.

Finally, we ran a preliminary test of the transducer to measure the speed of sound in air and in carbon dioxide. A simple setup was created using a Plexiglas box, where the

transducer would sit flat in the bottom of the box, as shown in Fig. 10. The microphone is held on a ring stand as before, but it is also placed through a layer of acoustic foam. The foam helps to partially acoustically isolate the box from the environment and to create a lid that, when sealed, prevents CO_2 from escaping the system.

In air, a 10 kHz pulse is sent from the transducer via a signal generator and the microphone records the response which is displayed on an oscilloscope. The oscilloscope reading can be seen in Fig. 11. The channel two (green) reading represents the signal sent from the signal generator to the transducer. The channel one (yellow) reading represents the signal received by the microphone. The time separation between the acoustic sent and the acoustic received signal is used in conjunction with the theoretical speed of sound at room temperature to determine the distance from the microphone to the transducer face. The distance from microphone to transducer is 21.1 cm.

A carbon dioxide atmosphere is created inside the box by placing a piece of dry ice in the corner and allowing it to sublimate. A vent tube through the acoustic foam allows for the air to be pushed out of the system as the CO_2 sublimates. The temperature inside the box is allowed to equilibrate until a thermocouple placed into the box via the vent tube reads the same as room temperature, 21°C. Again, a 10 kHz pulse is sent from the transducer to the microphone. The resulting oscilloscope reading is shown in Fig. 12. Again, the channel two (green) reading represents the signal sent from the signal generator to the transducer. The channel one (yellow) reading represents the signal received by the microphone.

Using the distance measurement from before, and the time separation, the velocity of sound in CO_2 is found to be 265 m/s. Theoretical speed of sound in CO_2 at 21°C is 269 m/s.

We attribute the difference in experimental and theoretical value to the fact that the sublimated CO_2 environment might not be completely pure, or the fact that there may be a small temperature gradient inside the box which shifts the speed of sound away from its actual value. Either way, the transducer is determined to work in a rudimentary carbon dioxide environment and is declared ready to be used in the next portion of the experiment.

A quick comment about the oscilloscope readings shown in Fig. 11 and Fig. 12: Note the presence of an electromagnetic signal in channel one. The acoustic signal appears later on the reading and is what is used to determine the time separation discussed above. The presence of a strong electromagnetic signal is not unexpected given the number of wires required to run the setup. We find that through proper grounding of the transducer and the equipment we can greatly reduce the amplitude of the electromagnetic signal.

Experimental Setup

With the transducer characterized and optimal operation settings known, we can proceed to develop an experimental setup for the measurement of speed of sound in different gases. We first look at the literature already existing on the topic. Several studies explore experimental designs that focus on two sets of stationary piezoelectric transducers[10] or two mobile transducers suspended on tracks inside of a resonance tube[11]. Due to the availability of materials and the design constraints of our transducer, we decide it is best to work with a stationary microphone and a mobile transducer inside of a steel pipe that will serve as our resonance tube.

Our experimental setup consists of a 4 foot long, 4 inch diameter steel pipe with a 1" wide flange on each end. One flange is designed to fit a long metal rod that attaches to the transducer. The rod allows the transducer's position inside the pipe to be changed. A wire fed through the flange allows for the transducer to be connected to the required electronics. The second flange is designed to hold the microphone so that it is on axis with the face of the transducer—in other words it sits directly in the center of the flange. A new microphone housing is constructed using aluminum pipe and an aluminum plug turned to the appropriate dimensions on a lathe. A schematic of the microphone and adapter plug is shown in Fig. 13. The microphone element is still a Knowles FG-3629 as was used in the characterization experiments.

Each flange is secured to the pipe via eight 15/16" bolts, tightened enough to seal the pipe from the outside environment. The flange which holds the transducer rod also has a gas inlet/outlet valve that is equipped with a quick release. This valve is used to evacuate the

system with a vacuum pump and to add air or carbon dioxide into the system from gas bottles. The vacuum pump used in this setup is model number VE115, with a flow rate of 1.8 CFM, purchased from Cynmar® Scientific Supplies and Equipment. The setup also has a Yellow Jacket® flutterless vacuum gauge attached to the end of the pipe nearest the flange with the transducer rod. A schematic of the setup is shown in Fig. 14 and a photograph is shown in Fig. 15.

In order to facilitate the transfer of gas from one side of the transducer to the other, four of the bolts used to tension the Mylar across the base are removed, as seen in Fig. 4. Bolts are removed at 90° angles from each other so that the tension across the plate remains as even as possible. Removing the bolts has no effect on the performance of the transducer, but it creates four holes in the base that gas can pass through. When the system is pumped down or refilled slowly, both the pipe in front of the transducer and the pipe behind the transducer are at equilibrium and we can be assured that the pressure reading on the gauge is the pressure of the system throughout the pipe.

A rough estimate of the distance between the transducer face and the microphone, l, can be calculated by measuring the distance, d, from the back flange to the end of the positioning rod, as shown in Fig. 16. The distance d is added to the width of the flange, w, and then that total is subtracted from the total length of the rod and transducer, D. This value will be a measurement of how much of the positioning rod is in the pipe. When this value is subtracted from the total length of the pipe, L, we are left with the distance from the front face of the transducer to the microphone, l. The exact distance l will be determined using the theoretical speed of sound in air, as described below.

Data Collection and Analysis in Air

Before the system is used with any pure gases, we first ran a test with air. The positioning rod is adjusted so that the transducer face is approximately 3.5 cm from the microphone. The test in air will be used along with the theoretical speed of sound in air, 343 m/s, to determine the exact distance from the transducer face to the microphone. The exact distance will then be used in further gas experiments.

To prepare the system for the measurement, it is evacuated to less than 1 inch Hg, an environment of 96.6% vacuum or higher. Air is allowed to enter the system from the room until the pressure inside the pipe is at 1 atm. To ensure that the temperature throughout the pipe is the same as the temperature inside of the room, the system sits for approximately an hour before any data is collected.

Once the system has reached equilibrium, data collection can begin. The signal is sent to the transducer using a Stanford Research Systems 2-Channel Dynamic Signal Analyzer—Model SR785. The signal used during the air tests is a swept sine wave with amplitude of 0.5 to 2.0 V. Data is recorded onto the signal analyzer using a logarithmic spacing, totaling 2047 data points for each frequency range. Frequency measurements range from 1 to 100 kHz in ten evenly spaced sets.

Data is collected onto a floppy disc and transferred to a computer and then converted into readable files using the Stanford Research Systems Data Viewer software. The data is saved in the form of ASCII files that can be accessed in the analysis system of choice. For these experiments, we analyzed our data in Microsoft Excel 2010.

When opened in Excel, the ASCII file has five columns of values: The frequency in Hertz, *X*, the magnitude of the signal in Volts, *Mag*, the phase shift in degrees, *P*, and the real, *R*, and imaginary, *I*, parts of the signal in Volts. We are really only concerned with the frequency and magnitude columns. A graph of frequency versus magnitude for the 1 to 11 kHz set is shown in Fig. 17.

It would be possible to pick out the peaks in the data using the mouse, but this is an unreliable method. We opt instead to use the function feature of Excel to create a function that will detect a peak and then display its frequency value or voltage value. The function centers around the fact that a peak in voltage would be indicated by the cells before and after the 'peak cell' having a lesser value. The function checks to see if the cell before and after the current cell is of a lesser value, and if they are, the frequency cell value is returned.

If the data is arranged in such a way that the magnitude column is in Column B on Excel and the frequency column is in Column A, the function to return the peak frequency looks as follows:

IF(AND(B18<B19, B20<B19), A19, "") (22)

This function will return the peak frequency value, or it will return nothing if the value is not at a peak. We can also modify the function to return the voltage values, as shown in Eq. 23.

IF(AND(B18<B19, B20<B19), B19, "") (23)

The other data sets are analyzed using the same functions. We condense the peak data into a single column, and now we can identify the first resonance frequency, which we will designate as n=1. It should be noted that the first resonance frequency is not necessarily

the first peak visible in the system. To ensure that we are selecting the actual first longitudinal resonance frequency and not a stray peak caused by radial or combination resonance, we use a rough distance measurement and an approximate value for the speed of sound in Eq. 14 to determine an approximate value for the first resonance frequency. Our selected peak should, obviously, be close to this value but not this value exactly.

For air, this resonance frequency, f_1, occurs at 4626 Hz. We can divide all of the peak data points into this frequency. Based on the relationship found in equation 5, we know that when f/f_1 returns an integer value we have reached a longitudinal resonance frequency for the system, assuming a constant speed of sound over the frequency range. The two longitudinal resonance frequencies found in the 1-11 kHz data set are indicated by red arrows in Fig. 17.

Values of resonance frequencies are recorded for the entire data range. When frequencies are plotted against their nodal number, *n*, they produce the graph that is shown in Figure 18. The data points can be fitted to a straight line in Excel, but we prefer to use the method of linear fitting that calculates the slope of the data by hand[12]. Sample calculations for linear fits and error propagation can be seen in Appendix B. The slope of this data is found to be 4615 ± 8 Hz. We know that the speed of sound in air is 343 m/s, and using the relationship in equation 5, we find that the length of the pipe between the transducer face is 3.716 ± 0.006 cm.

If we return to Fig. 17 we see that there are many more peaks than the two longitudinal resonance frequencies indicated by the red arrow. Several of these peaks represent the

cylindrical resonance frequencies of the pipe. These peaks are indicated by blue arrows on Fig. 17.

What about the peaks that do not fit the purely longitudinal or purely cylindrical resonance modes described above? These peaks, highlighted by green arrows on Fig. 17, are resonance frequencies that are a combination of longitudinal and cylindrical resonances. In other words, they are frequencies given by Eq. 19.

Frequencies that are not combination resonances, cylindrical resonances, or the purely longitudinal resonances may emerge later in the data sets, but our main concern lies with the frequencies described above. With the exact distance between the transducer face and the microphone determined and the system working well in air, we are now ready to examine the speed of sound in other gases.

Data Collection and Analysis in Carbon Dioxide

The second gas we will explore is pure carbon dioxide, CO_2. Carbon dioxide is a cheap, relatively inert, and usually harmless gas when handled correctly, so it is ideal for use in our experiment.

Collecting resonance data in CO_2 is similar to collecting data in air. The system is evacuated to less than 1 inch Hg, an environment of 96.6% vacuum or higher. Using a dry, high quality, CO_2 tank, the system is filled to 1 atmosphere. Gas expanding from the tank will cool, so the system must be allowed to equilibrate and return to room temperature. It is normal for the pressure to drop slightly during this period of equilibration. Before data is collected, the pressure gauges should be checked and gas should be allowed into the system to compensate for the pressure lost during equilibration.

Again the signal analyzer is used to send a swept sine wave signal. Data is recorded using a linear spacing, totaling 2047 data points for each frequency range. Again, frequency measurements range from 1 – 100 kHz, in ten evenly spaced sets. Due to its molecular structure, carbon dioxide is a gas which attenuates energy incredibly quickly.[13] After a certain frequency peak, approximately 30 kHz, the amplitude of the sound signal that reaches the microphone from the transducer face begins to decay. To combat this signal loss, we vary the voltage from the source across the frequency range. Voltage values used and their corresponding frequency ranges are recorded in Table 1.

Data is analyzed exactly as it is done for air. A graph of the first data set, 1 – 11 kHz, can be seen in Fig. 19. As before, we have identified the longitudinal resonance modes (indicated by red arrows), cylindrical resonance modes (indicated by blue arrows), and resonance

modes that result as a combination of longitudinal and cylindrical components (indicated by green arrows).

The f_1 for CO_2 is found to be 3649 Hz. A graph of frequency versus nodal number is presented in Fig. 20. The slope of the resulting line is calculated using the same linear fit method, and it is found to be 3679 ± 9 Hz. Using the length determined by the run in air, the speed of sound in CO_2 is experimentally determined to be 273.4 ± 0.8 m/s.

Reported values[14] indicate that the speed of sound in CO_2 at 20°C actually varies slightly depending on the frequency of the sound. At the low end (approximately 5 kHz) the sound speed is approximately 269 m/s. At the high end (100 kHz and above) the sound speed can be as fast as 279 m/s. Several attempts were made to resolve the change in sound speed across our frequency range[15], but our experimental setup lacks the precision necessary to see these small changes. Our experimental value, however, falls at a reasonable median of the two expected values.

Data Collection and Analysis in Helium

The third gas used in our experimental system, helium, is inert and has the advantage of being a monatomic gas with incredibly simple molecular structure. Helium gas should not have the same issues that carbon dioxide (a complex, diatomic gas) did with attenuation at high frequencies.

As with CO_2 and air, the experimental setup is first evacuated to less than 1 inch Hg, an environment of 96.6% vacuum or higher. The system is filled and then allowed to sit for an hour or more to equilibrate with room temperature before data is collected. As before, our signal generator sends a swept sine wave, and data is collected linearly with 2047 data points per frequency range, spanning 1 – 100 kHz in ten evenly spaced sets.

The data for the second frequency range, which is where the first resonance frequency occurs, is shown in Fig. 21. As with air and CO_2, we identify longitudinal resonance peaks on the graph with a red arrow, cylindrical resonance peaks with a blue arrow, and combination resonance peaks with a green arrow. The first longitudinal resonance frequency in helium occurs at 12722 Hz.

A graph of the resonance frequencies versus nodal number can be seen in Fig. 22 and is calculated to have a slope of 12778 ± 127 Hz. From this value our calculated speed of sound in helium gas 950 ± 10 m/s. The theoretical values for the speed of sound in helium range from 927 m/s[16] to 1010 m/s[17], and our value fits nicely within these parameters. It should be noted that the speed of sound in helium has a larger error associated with it than the speed of sound in carbon dioxide. Is this due to a failing in our system?

In short, no. The large value for f_1 in helium means that there are seven data points available in the 1 – 100 kHz frequency sweep. In CO_2, we are able to collect twenty-six data points. An increase in the number of available data points usually increases the precision of the overall answer. If we were able to obtain resonance frequency data above 100 kHz we would increase the precision of our answer. Unfortunately we are limited to the 100 kHz upper limit on the signal generator and, as determined previously, our signal generator and microphone operate best below the 100 kHz limit.

Data Collection and Analysis in Gas Mixtures

Having tested the experimental setup with three pure gases, we can move now to testing the system's performance using binary gas mixtures. The true power of having a simple method of determining the speed of sound in a gas lies in being able to correlate that sound speed back to the environment where the sound is traveling. One can easily see the usefulness in this ability. Imagine constructing a sensor that can measure the speed of sound in a given length of pipe, or that is designed to resonate at a given frequency corresponding to a certain environment. Such a device could be a rudimentary warning system for detecting the presence of dangerous gases in air.

With this in mind, we want to prove that our system is capable of detecting the changes in speed of sound that arise from varying the composition of the gas mixture in the pipe. For a binary mixture, the relationship between speed of sound and the composition of the gas is found by first looking at how we can define the speed of sound:

$$c = \sqrt{\gamma_{mix}\mathbb{R}_{mix}T} \tag{24}$$

where T is the temperature of the gas in Kelvin, γ_{mix} is the ratio of specific heats for the mix, and $\mathbb{R}_{mix}$is the ratio of the molar gas constant for the mix. The binary mixture can be treated as a linear combination of the two components, which means that we define

$$\mathbb{R}_{mix} = \frac{R}{m_1(1 - X_{12}) + m_2(X_{12})} \tag{25}$$

where R is the gas constant 8.314 J/mol-K, X_{12} is the partial pressure of component 1 in component 2, and m_1 and m_2 are the molecular weights of the two components of the mixture. We also know

$$\gamma_{mix} = \frac{C_{p1}(1 - X_{12}) + C_{p2}X_{12}}{C_{v1}(1 - X_{12}) + C_{v2}X_{12}} \tag{26}$$

This makes the overall theoretical statement for the speed of sound in a binary mixture

$$c = \sqrt{\left(\frac{R}{m_1(1 - X_{12}) + m_2(X_{12})}\right)\left(\frac{C_{p1}(1 - X_{12}) + C_{p2}X_{12}}{C_{v1}(1 - X_{12}) + C_{v2}X_{12}}\right)T} \tag{27}$$

Using Eq. 27, we can create a prediction for what the speed of sound should be over a range of partial pressures in a particular mixture. We can then compare these values with values collected experimentally.

A Mixture of CO_2 and Helium

To begin with, we will examine a mixture of the two gases which have the largest speed difference, and thus the most drastic change across the partial pressure range. The system is prepared almost exactly as before. The only difference being instead of filling the system immediately to 1 atm with the gas of choice, we fill the system with a partial pressure of one gas, and then fill the rest of the way with the second gas. The pressure gauge on the system is marked with 15 ticks from 1 atm to vacuum, which makes filling partial pressures considerably easier. The partial pressures tested, along with the tick marks on the gauge used to fill the system, are recorded in Table 2.

The system must still be allowed to sit for an hour before data is collected. The signal generator sends a swept sine wave and collects data linearly for a total of 2047 data points per run. Data is collected along the 1 – 100 kHz frequency range in ten evenly spaced sets, as described above. Because we are dealing with CO_2 the voltage is varied across the data collection to make up for the attenuation of the sound over the frequency range.

Data is analyzed in the same way as it was for the pure gases. As before, we can identify longitudinal, cylindrical, and combination resonance frequencies in the data. The longitudinal resonance frequencies are used to calculate the speed of sound in the mixture. A graph of the frequency versus nodal number for each of the partial pressure mixtures is presented in Fig. 23. The calculated slope and speed of sound for each mixture is presented in Table 3.

These data points are then plotted in conjunction with the theory given by equation 20. The resulting graph is shown in Fig. 24, with the theory given by the red dashed line. Our

experimental data fits the theory incredibly well. At high helium concentrations the values shift slightly lower than the theory predicts, but as stated above the accepted value for the speed of sound in helium covers a wide range (900 – 1000 m/s).

A Mixture of CO_2 and Air

We now have proof of concept. Our experimental setup can determine the speed of sound in a mixture of helium and carbon dioxide with great accuracy. However, the sound speed difference between helium and CO_2 is very large. Can our setup distinguish between two gases that have a much closer speed of sound? Air and CO_2, with their sound speeds of 343 m/s and 273 m/s respectively are ideal for testing this.

However, there is another reason why we are interested in mixtures of air and CO_2. The air we breathe is a combination of multiple gases, yet our body only uses the oxygen in the air that we inhale. Carbon dioxide is normally present in the air in a concentration of 385 ppm[18]. CO_2 is an asphyxiant gas, which means that, while it is classified as non-toxic, in high concentrations it can displace the air in the human lungs and decrease oxygen uptake causing asphyxiation and ultimately death. Table 4 shows the values of CO_2 concentrations that have negative effects on the human body[19].

It is important to be able to accurately measure the concentration of CO_2 in the environment, or to be able to notify anyone in the vicinity when the CO_2 level becomes dangerous. Currently sensors exist to monitor CO_2 levels using infrared light tuned to detect CO_2[20]. If our system could detect CO_2 concentrations using an acoustic signal the idea could be transferred to a sensor that may be useful in industrial, recreational, or education environments.

The air and CO_2 mixtures are tested following the exact procedure defined for the CO_2 and helium mixtures. The resulting plots of frequency versus nodal number for each partial pressure are presented in Fig. 25. The calculated slopes and speeds of sound are shown in

Table 5 and the theoretical data plotted alongside the experimental points is presented in Fig. 26.

A look at Fig. 26 gives the impression that our theory and our data do not match; all of our experimental values are below where the theory would predict them to be. Is this the system falling short, or is this a mistake on our part?

We may first believe that we have made a critical error in our theory. The values used for C_p, C_v, and m in equation 27 are for dry air. If we were drawing air from a gas tank this claim would be accurate. As it stands, our air is humid and the values of specific heats and molar mass must be adjusted accordingly. We can treat the air as a linear combination of air and water molecules, with the mole fraction being given by the percentage of humidity.

A corrected graph of theoretical versus experimental speeds of sound in carbon dioxide and air mixtures is shown in Fig. 27. Typical outdoor relative humidity level in Arkansas in July is 60%[21]. We do not have a humidity sensor inside of the system or in our lab so we opt instead to alter the value for the humidity until the theory fits the data. A value of approximately 2% humidity causes the data and theory to correlate. This is much lower than typical indoor relative humidity[22] and would be an almost impossible environment to achieve. This leads us to believe that the error must lie somewhere within the system or the theory.

Still, our system was capable of detecting the small changes in speed of sound that arise from mixtures of CO_2 and air, so this experiment is still somewhat of a success. To create a more accurate design, we should incorporate a desiccant into the tube or use a dry air tank.

A Mixture of Helium and Air

For completeness, we test the speed of sound in mixtures of helium and air. Like CO_2 helium is an asphyxiant gas and when present at high levels in an environment can cause asphyxiation and death. However, death by helium inhalation is rare and usually arises from situations where helium has been inhaled directly from the tank, with the high pressure being more dangerous than the chemical makeup of the gas itself[23].

Experimental procedure for helium and air follows the exact procedure detailed in the CO_2 and helium and CO_2 and air sections. The resulting plots of frequency versus nodal number for each of the partial pressures of helium in air are presented in Fig. 28. The calculated slopes and speeds of sound are shown in Table 6 and the theoretical data plotted alongside the experimental points is presented in Fig. 29.

The values in Fig. 29 appear to match the theory pretty well. However, in the last section we had to make a correction for the fact that we were working with dry air rather than humid air. For consistency, we need to make a similar correction in this mixture, but the change is less apparent because the scale of the sound speed change is much larger—from 343 m/s to 950 m/s rather than 343 m/s to 273m/s. A humidity corrected graph, with the correction performed as described previously, is shown in Fig. 30. Again, a value of 2% humidity is used, but 2% humidity is extremely low and is not a reasonable approximation. We believe a more correct speed of sound graph could be achieved by using a desiccant inside of the experimental setup or by using a dry air tank rather than the air inside of the room.

Conclusion

Throughout the course of our research project, we have designed and manufactured an experimental setup that effectively measures the speed of sound in various pure gases. The setup can also measure the speed of sound of gas mixtures accurately across large speed gaps like those seen in helium and air and helium and CO_2 mixtures and small speed gaps like those seen in a CO_2 and air mixture. With some perfecting and minimizing, the procedure and devices used in this experiment could be incorporated into a sensor that uses acoustics to measure and monitor the CO_2 concentration in the environment. The setup is also relatively easy to operate and could easily be incorporated into an undergraduate upper division physics or chemistry laboratory if the instructor desired a simple exploration of sound speeds in various media.

Future work on this project will revolve around adapting the system to test a wide variety of gases and mixtures effectively. A more accurate system for positioning the transducer face and measuring the distance from the transducer face to the microphone will increase the accuracy of our system. The Knowles microphone used in this experiment worked well, but a microphone that has a better response at high frequencies and a faster response time would allow for an increase in the amount of data that could be collected. A final improvement to the system would be finding a signal generator that could generate frequencies higher than 100 kHz. Perhaps with these adjustments we could resolve the speed of sound change across the frequency range in carbon dioxide, or make accurate sound attenuation measurements in gases.

It may also be desirable to pursue a method of data analysis that does not rely on knowing the approximate speed of sound in a mixture to determine where the approximate first resonance frequency value should be. The peaks predicted by Eq. 19 seem to appear pretty regularly in the data. One could see the creation of a computer program that fits the theoretical predictions for peaks to the actual data collected by altering the value for the speed of sound. This would eliminate the need for initial guesswork and the comparison of the frequency versus nodal number to determine *c*. If this method could be developed, the system could be used to identify the speed of sound in unknown gases or binary gas mixtures.

As it stands, the experimental setup is useful and accurate. It holds a lot of promise when it comes to future work, and we look forward to pursuing the exploration of acoustic behavior of gases.

Acknowledgements

The work presented above was funded by two Student Undergraduate Research Fund grants from the Arkansas Department of Higher Education, and a Student Research Fund grant from the University of Central Arkansas College of Natural Science and Mathematics. The author would like to personally acknowledge Dr. William Slaton for his invaluable assistance and guidance in all aspects of the project through his role as research advisor, and Dr. Stephen Addison for his advice on the development of the system and his role as editor of the thesis. Special thanks to the UCA Department of Physics and Astronomy for the opportunity to participate in undergraduate research and develop the project from the ground up. It has been a true blessing and an amazing learning experience.

References

[1] Kinsler, Lawrence E., Frey, Austin R., Coppens, Alan B., and Sanders, James V. *Fundamentals of Acoustics.* Chapter 5.5: The Linear Wave Equation. 4th Ed, Wiley & Sons, 2000.

[2] Kinsler, Lawrence E., Frey, Austin R., Coppens, Alan B., and Sanders, James V. *Fundamentals of Acoustics.* Chapter 9.3: The Cylindrical Cavity. 4th Ed, Wiley & Sons, 2000.

[3] Kinsler, Lawrence E., Frey, Austin R., Coppens, Alan B., and Sanders, James V. *Fundamentals of Acoustics.* Appendix A5: Bessel Functions: Tables, Graphs, Zeros, and Extrema. 4th Ed, Wiley & Sons, 2000.

[4] We used the ke!+san Online Calculator for Bessel Function Zeros to determine the necessary solutions to the Bessel function. The calculator is accessible at: http://keisan.casio.com/exec/system/1180573472

[5] Shields, F. Douglas, H. e. Bass, and L. N. Bolen. "Tube method of sound-absorption measurement extended to frequencies far above cutoff." *Journal of the Acoustical Society of America*. Vol. 62, No. 2, August 1977.

[6] Kinsler, Lawrence E., Frey, Austin R., Coppens, Alan B., and Sanders, James V. *Fundamentals of Acoustics.* Chapter 14.3(a): The Electrostatic Transducer (Reciprocal). 4th Ed, Wiley & Sons, 2000. The circuit design shown here was modified by Dr. Stephen Addison, UCA and this modified design was used as a basis for the transducer circuit constructed.

[7] All data is not presented in the paper. A digital copy of all data discussed in this paper is available from the UCA Department of Physics and Astronomy.

[8] Microphone specs are available from the manufacturer, or in the technical document available here: http://www.newark.com/knowles-acoustics/fg-3629-p16/microphone-33db-omni-10khz/dp/95C0254

[9] Kinsler, Lawrence E., Frey, Austin R., Coppens, Alan B., and Sanders, James V. *Fundamentals of Acoustics.* Chapter 7.4(a): Axial Response of a Plane Circular Piston. 4th Ed, Wiley & Sons, 2000.

[10] Petculescu, Andi. "A prototype acoustic gas sesnsor based on attenuation (L)." *Journal of the Acoustical Society of America.* 120 (4), October 2006.

[11] Ejakov, Sally G. "Acoustic attenuation in gas mixtures with nitrogen: Experimental data and calculations." *Journal of the Acoustical Society of America*. 113 (4) Pt. 1. April, 2003.

[12] Taylor, John. *An Introduction to Error Analysis: The Study of Uncertainties in Physical Measurements*. 2nd Ed, University Science Books, 1996.

[13] Kinsler, Lawrence E., Frey, Austin R., Coppens, Alan B., and Sanders, James V. *Fundamentals of Acoustics.* Chapter 8.6: Molecular Thermal Relaxation. 4th Ed, Wiley & Sons, 2000.

[14] Kinsler, Lawrence E., Frey, Austin R., Coppens, Alan B., and Sanders, James V. *Fundamentals of Acoustics.* Chapter 8.6, Figure 8.6.1. 4th Ed, Wiley & Sons, 2000.

[15] An account of procedures attempted to resolve the change in sound speed is given in Appendix C.

[16] Value for the speed of sound in helium found at HyperPhysics: http://hyperphysics.phy-astr.gsu.edu/hbase/sound/souspe.html#c4

[17] Value for the speed of sound in helium found at: http://mysite.du.edu/~jcalvert/phys/helium.htm

[18] Information about the gases used in the experiments, including air, is found at an AirLiquide Encyclopedia. Here, gases can be searched by name or by the UN Transportation Code that is found on their cylinders. The URL for the encyclopedia is: http://encyclopedia.airliquide.com

[19] Lambertsen, Christian J. (1971). "Carbon Dioxide Tolerance and Toxicity". Environmental Biomedical Stress Data Center, Institute for Environmental Medicine, University of Pennsylvania Medical Center (Philadelphia, PA). IFEM Report No. 2–71.

[20] An example of and IR CO_2 sensor can be found at E+E Elektronik: http://www.epluse.com/en/products/co2-measurement

[21] This statement is made on the basis checking comprehensive weather data for several days: http://www.wunderground.com.

[22] CenterPoint Energy: Humidity & The Indoor Environment accessible at: http://www.centerpointenergy.com/staticfiles/CNP/Common/SiteAssets/doc/Humidity_indoor_environ[1].pdp

[23] Engber, Daniel. “Stay Out of That Balloon! The Dangers of Helium Inhalation.” *Slate Online*. 13 June, 2006.

Appendix A – Tables and Figures

Data Set	Frequency (kHz)	Signal Amplitude (V)
1	1-11	0.5
2	10-20	0.5
3	19-30	0.5
4	29-40	1.0
5	39-50	1.0
6	49-60	1.5
7	59-70	2.0
8	69-80	2.0
9	79-90	2.5
10	89-100	5.0

Table 1: Frequency and signal amplitude for each of the data runs in CO_2.

Partial Pressure He (atm)	Partial Pressure CO_2 (atm)	Tick Marks He	Tick Marks CO_2
1.0	0.0	0	15
0.9	0.1	1.5	13.5
0.8	0.2	3	12
0.7	0.3	4.5	10.5
0.6	0.4	6	9
0.5	0.5	7.5	7.5
0.4	0.6	9	6
0.3	0.7	10.5	4.5
0.2	0.8	12	3
0.1	0.9	13.5	1.5
0.0	1.0	15	0

Table 2: Partial pressures and tick marks used to fill the system with a binary gas mixture.

Partial Pressure He (atm)	Calculated Slope (Hz)	Speed of Sound (m/s)
1.0	12778 ± 127	950 ± 10
0.9	9020 ± 53	670 ± 4
0.8	7321 ± 49	544 ± 4
0.7	6643 ± 30	493 ± 2
0.6	5572 ± 18	414 ± 2
0.5	5054 ± 20	375.6 ± 1.6
0.4	4834 ± 17	359.2 ± 1.4
0.3	4339 ± 25	322.5 ± 1.9
0.2	4023 ± 10	299.0 ± 0.9
0.1	3812 ± 42	283 ± 3
0.0	3679 ± 9	273.4 ± 0.8

Table 3: Calculated slopes and speeds of sound for mixtures of helium and CO_2.

% CO_2 in Inspired Air	Effect of Exposure to CO_2 on the Body	
	Duration of Exposure	Effect
0.03	Lifetime	Normal atmosphere
0.5	Lifetime	No detectable limitations
1.0	Lifetime	
1.5	> 1 month	Mild respiratory stimulation
2.0	> 1 month	
2.5	> 1 month	
3.0	> 1 month	Moderate respiratory stimulation
3.5	> 1 week	
4.0	> 1 week	Moderate respiratory stimulation, exaggerated respiratory response to exercise
4.5	> 8 hours	
5.0	> 4 hours	Prominent respiratory stimulus, exaggerated respiratory response to exercise
5.5	> 1 hour	
6.0	> 30 minutes	Prominent respiratory stimulus, exaggerated respiratory response to exercise, beginnings of mental confusion
6.5	> 15 minutes	
7.0	> 6 minutes	Dyspnea and mental confusion, leading to death

Table 4: Negative effects of CO_2 concentrations on the body.

Partial Pressure CO_2 (atm)	Calculated Slope (Hz)	Speed of Sound (m/s)
1.0	3679 ± 9	273.4 ± 0.8
0.9	3654 ± 11	271.5 ± 0.9
0.8	3766 ± 18	279.9 ± 1.4
0.7	3802 ± 8	282.6 ± 0.8
0.6	3906 ± 15	290.3 ± 1.2
0.5	3957 ± 15	294.1 ± 1.2
0.4	4139 ± 13	307.6 ± 1.1
0.3	4215 ± 15	313.3 ± 1.2
0.2	4374 ± 10	325.1 ± 0.9
0.1	4450 ± 11	330.7 ± 0.9
0.0	4615 ± 8	343

Table 5: Calculated slope and speed of sound for partial pressures of CO_2 in air.

Partial Pressure He (atm)	Calculated Slope (Hz)	Speed of Sound (m/s)
1.0	12778 ± 127	950 ± 10
0.9	10299 ± 92	765 ± 7
0.8	8326 ± 52	619 ± 4
0.7	7563 ± 32	562 ± 3
0.6	6864 ± 34	510 ± 3
0.5	6176 ± 13	459.0 ± 1.3
0.4	5914 ± 20	439.5 ± 1.7
0.3	5415 ± 15	402.5 ± 1.3
0.2	5173 ± 11	384.4 ± 1.1
0.1	4826 ± 12	358.7 ± 1.1
0.0	4615 ± 8	343

Table 6: Calculated slopes and speeds of sound for varying partial pressures of helium in air.

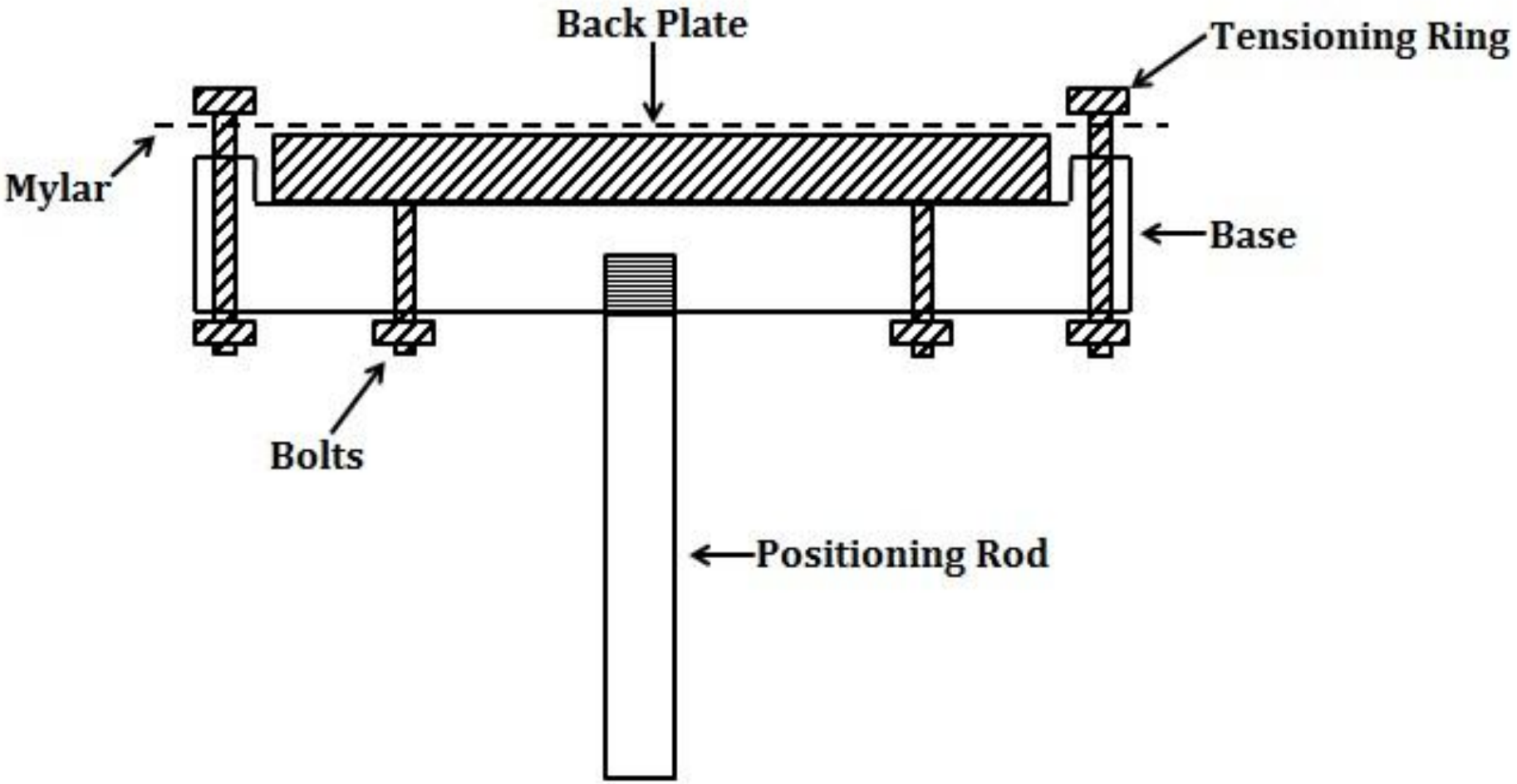

Figure 1: Sideways schematic of transducer design

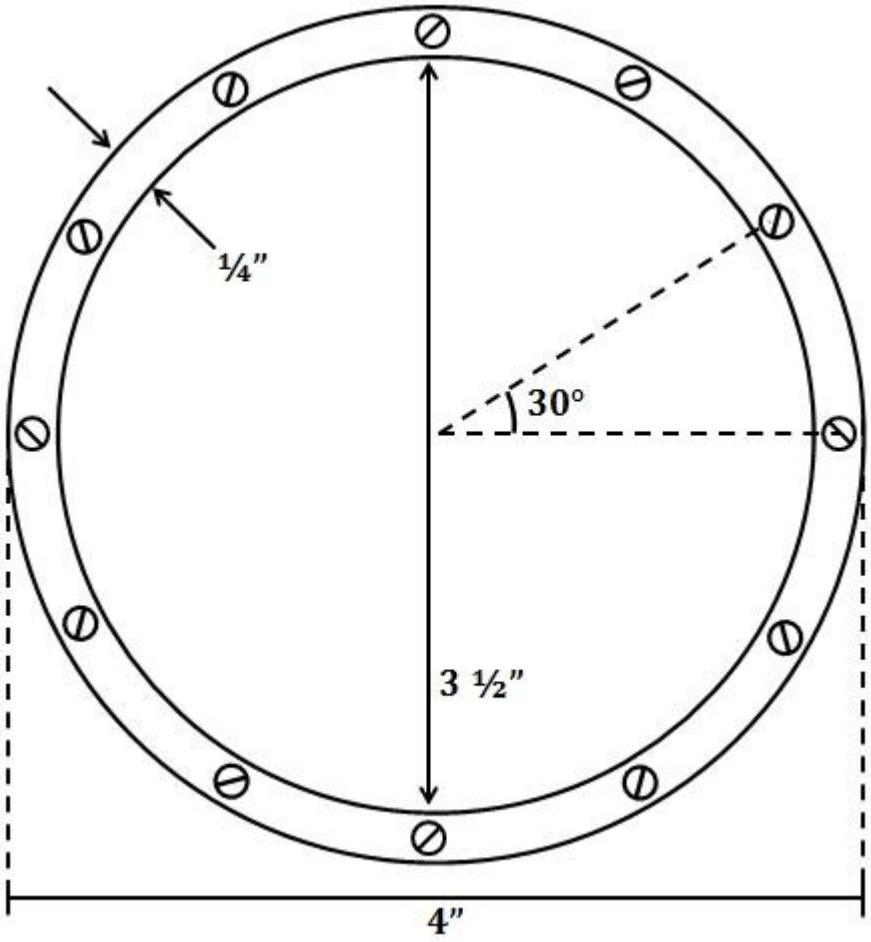

Figure 2: Bolt position on brass tensioning ring

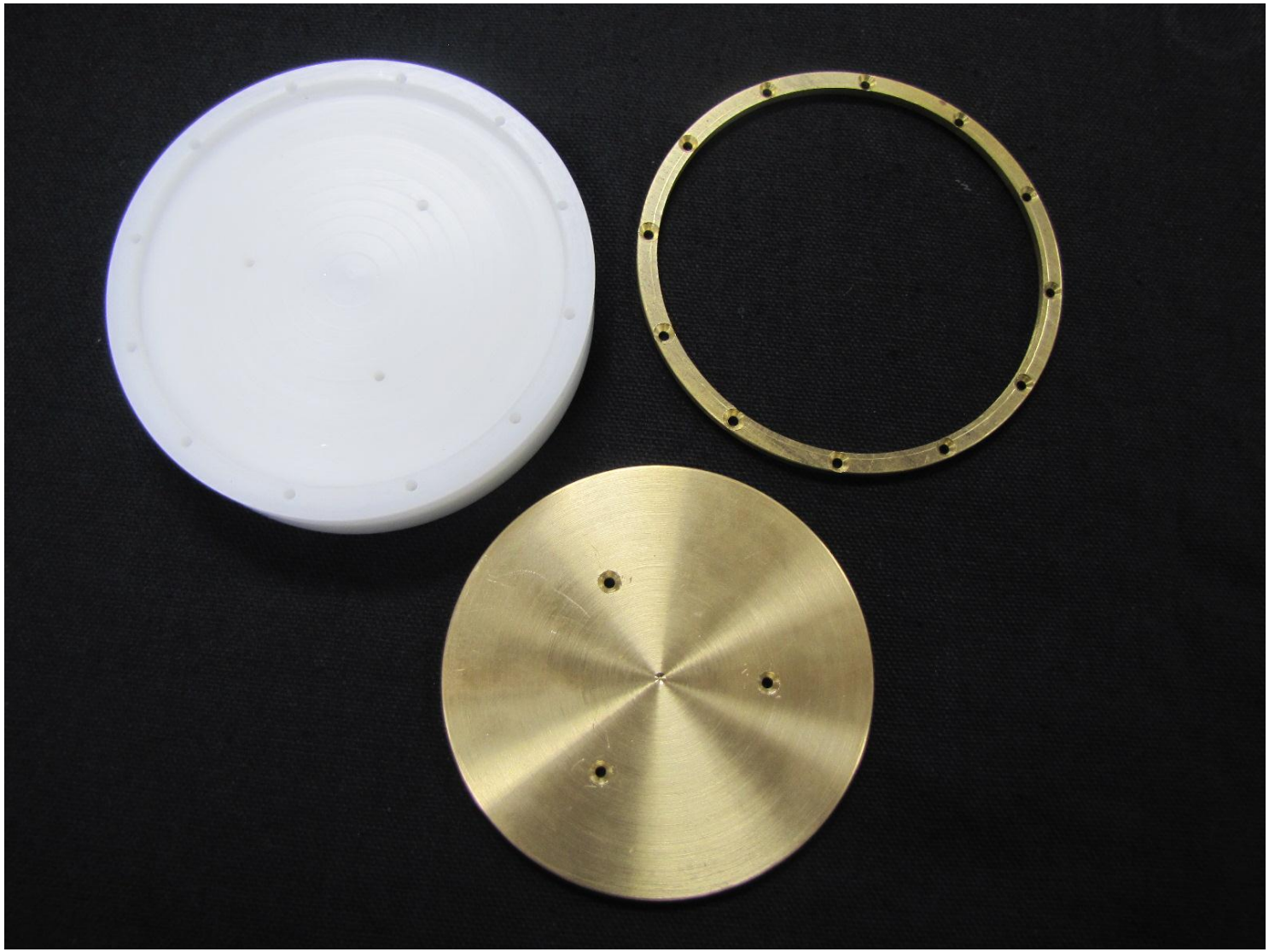

Figure 3: Disassembled transducer. Clockwise from left: Delrin plastic base, brass tensioning ring, brass backing plate.

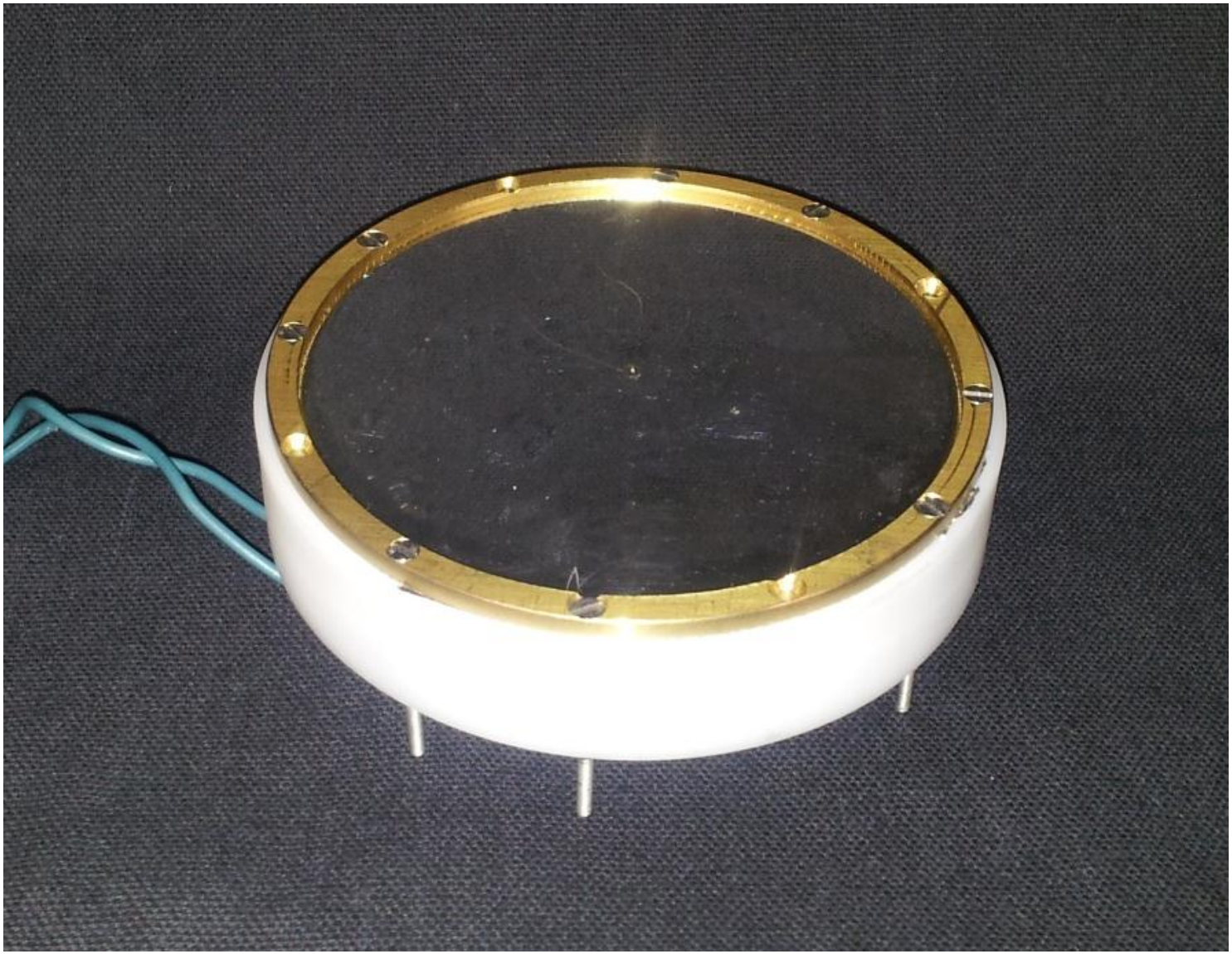

Figure 4: Assembled transducer with electrical connections to the bolts beneath the base.

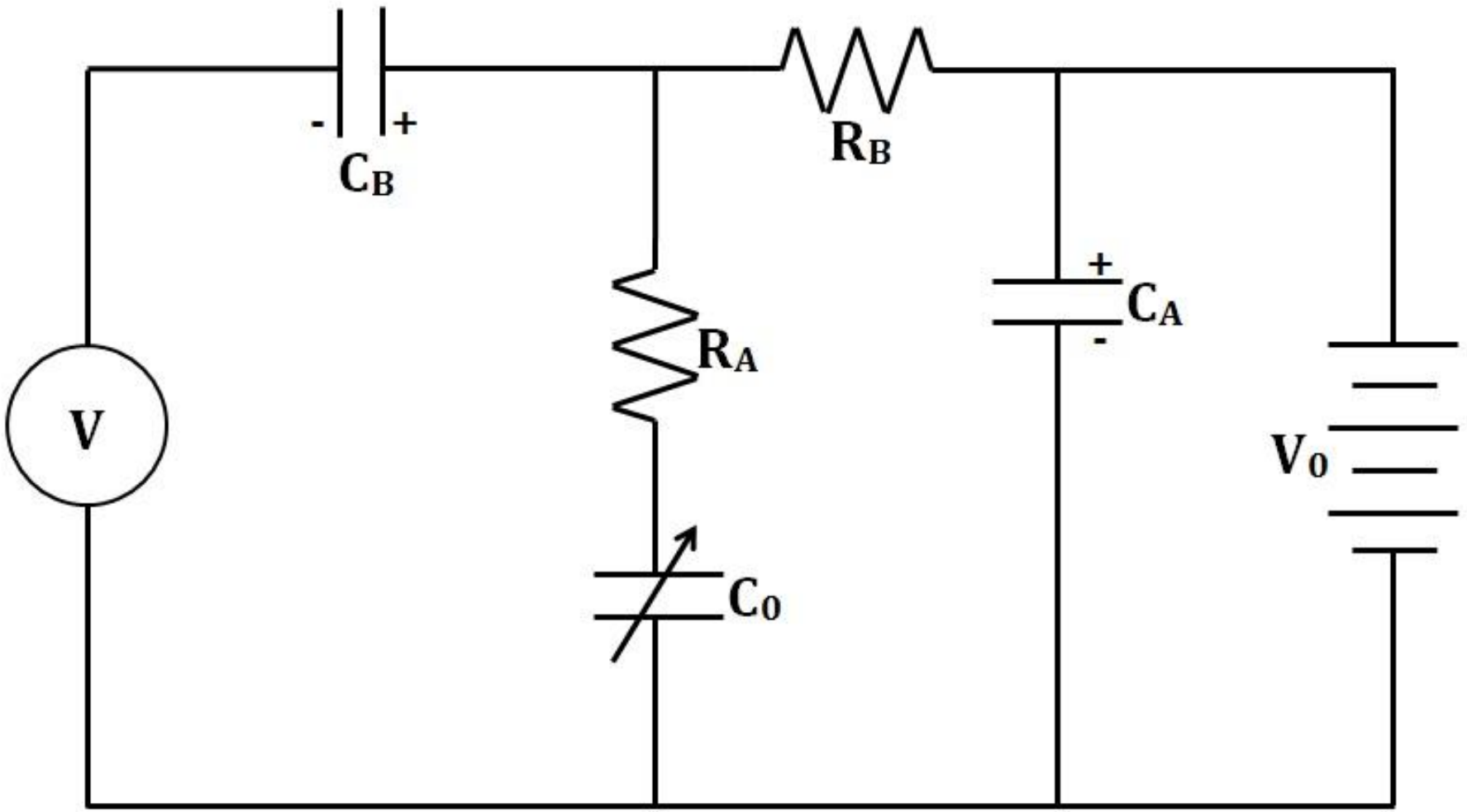

Figure 5: Voltage adder circuit for the transducer.

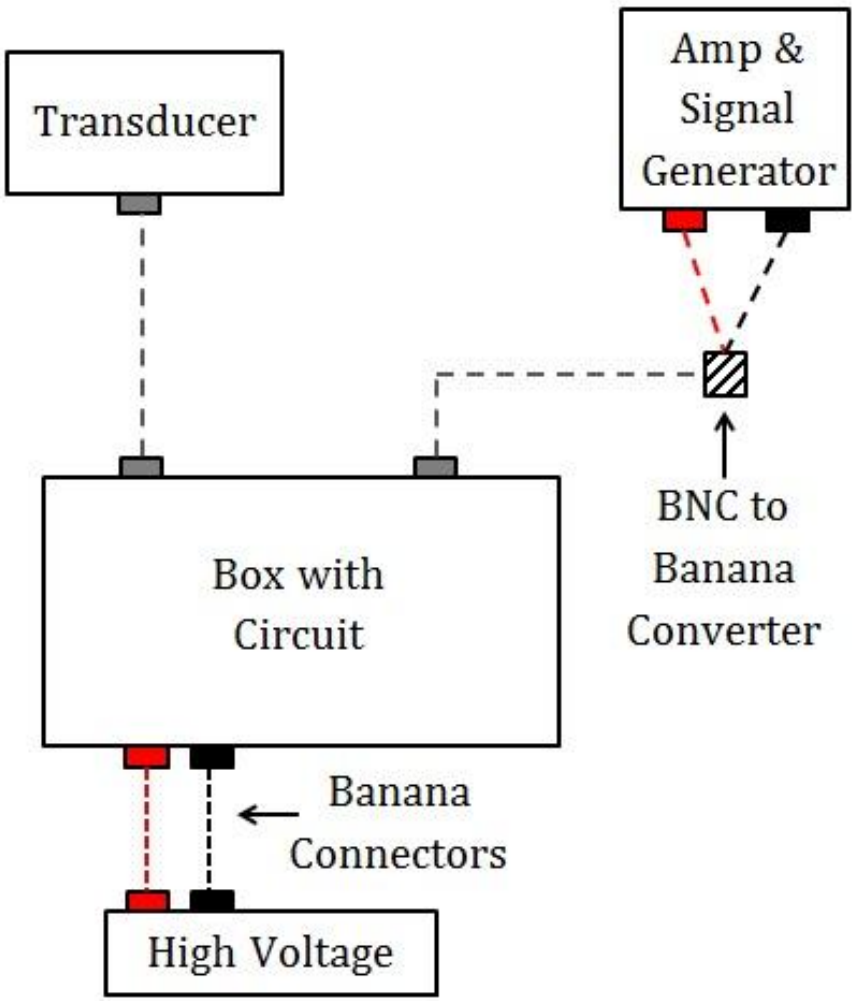

Figure 6: Electronic hookup from the circuit box to equipment.

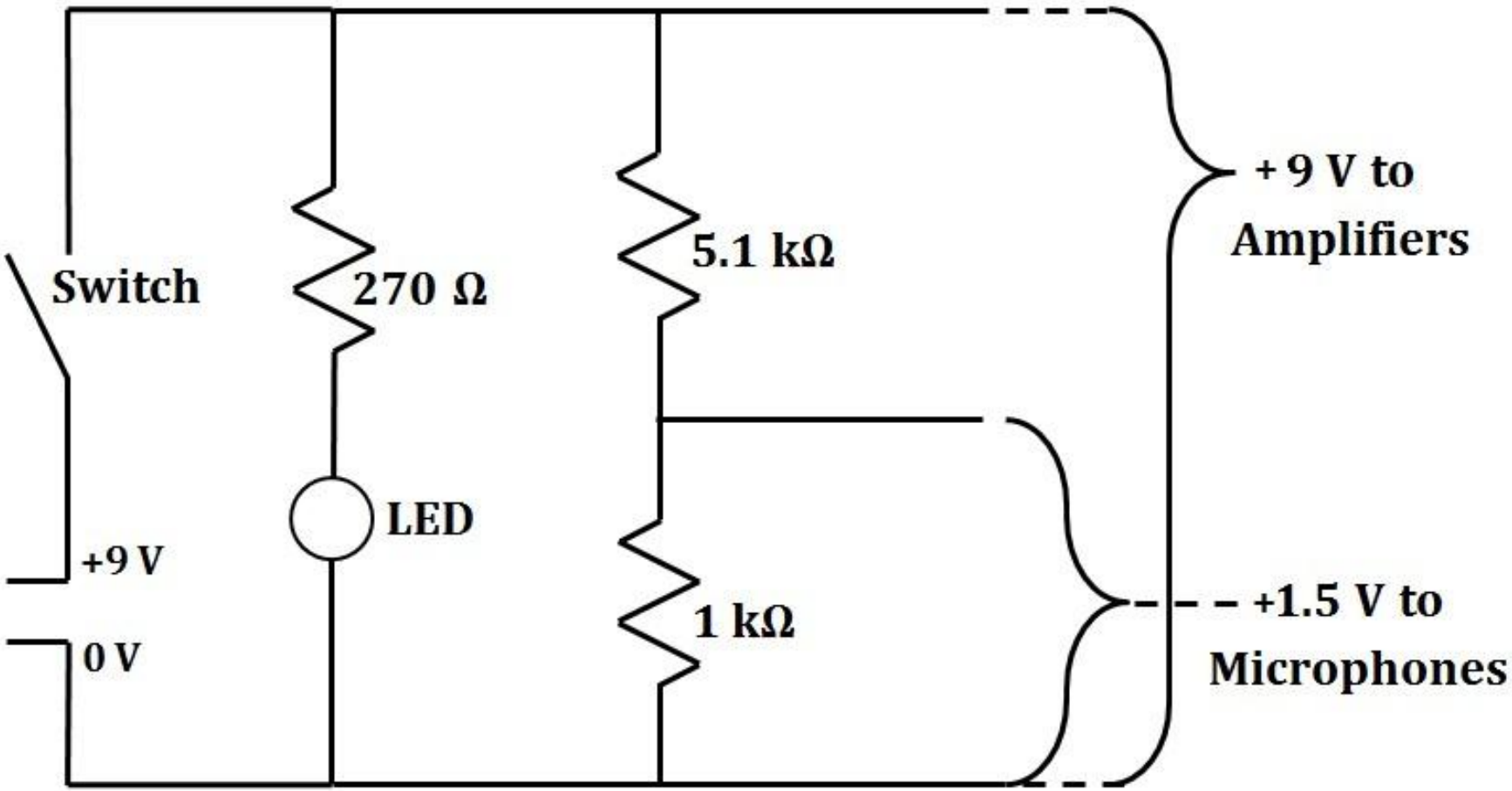

Figure 7: Microphone power and amplification circuit.

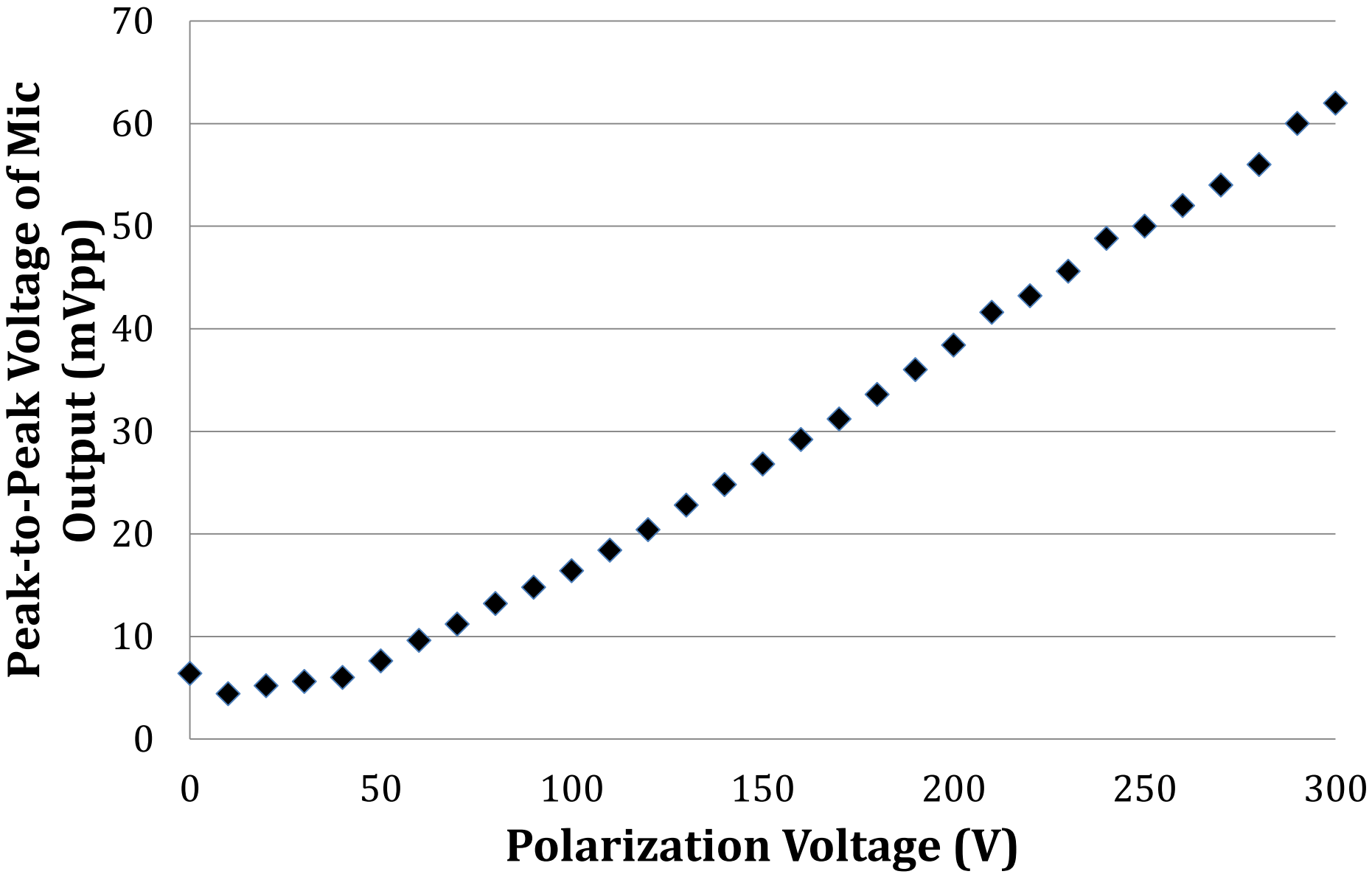

Figure 8: Voltage output for varying DC polarization bias.

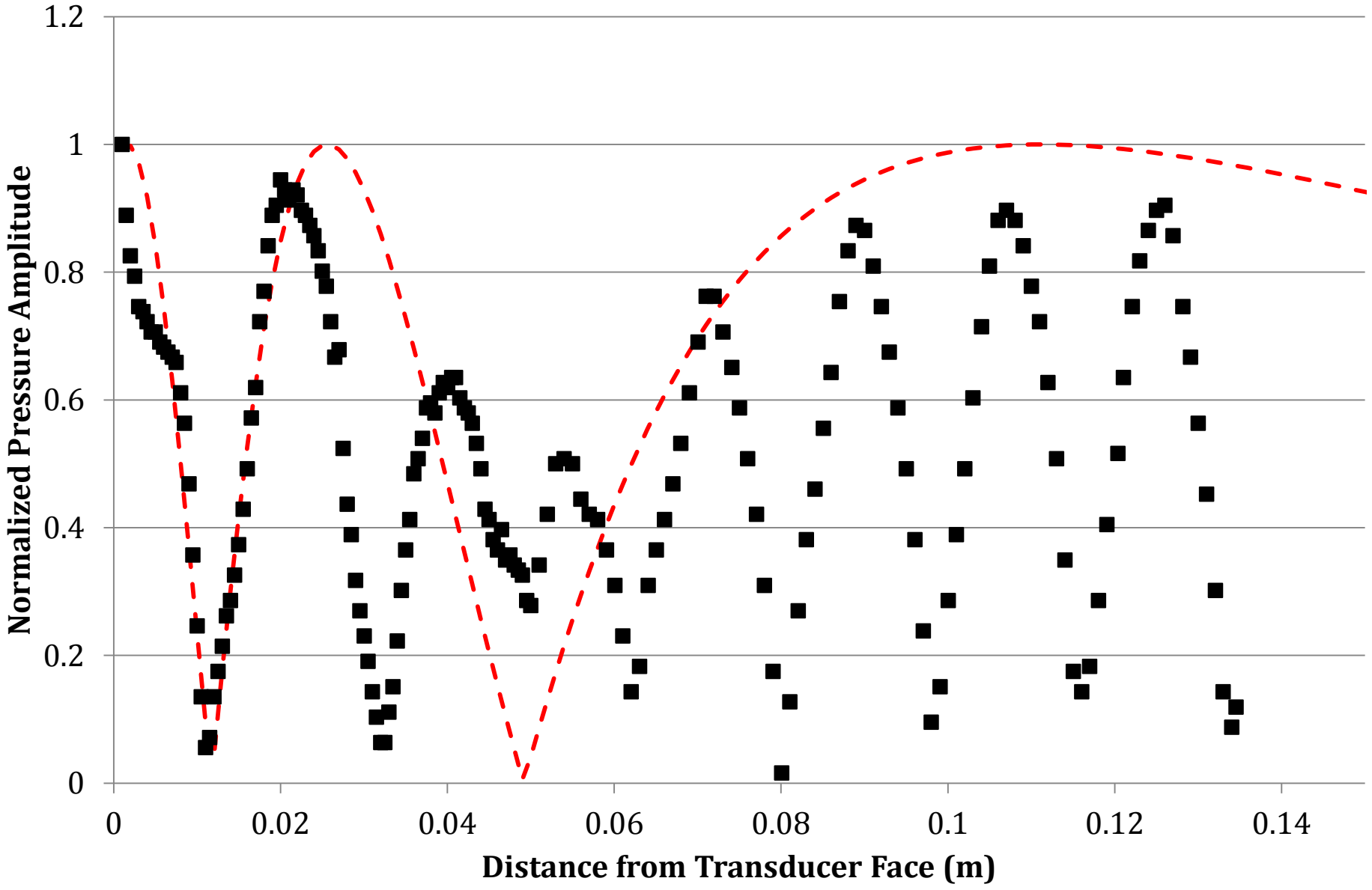

Figure 9: Comparison of near-field theory (red dashed line) with experimental data (black points).

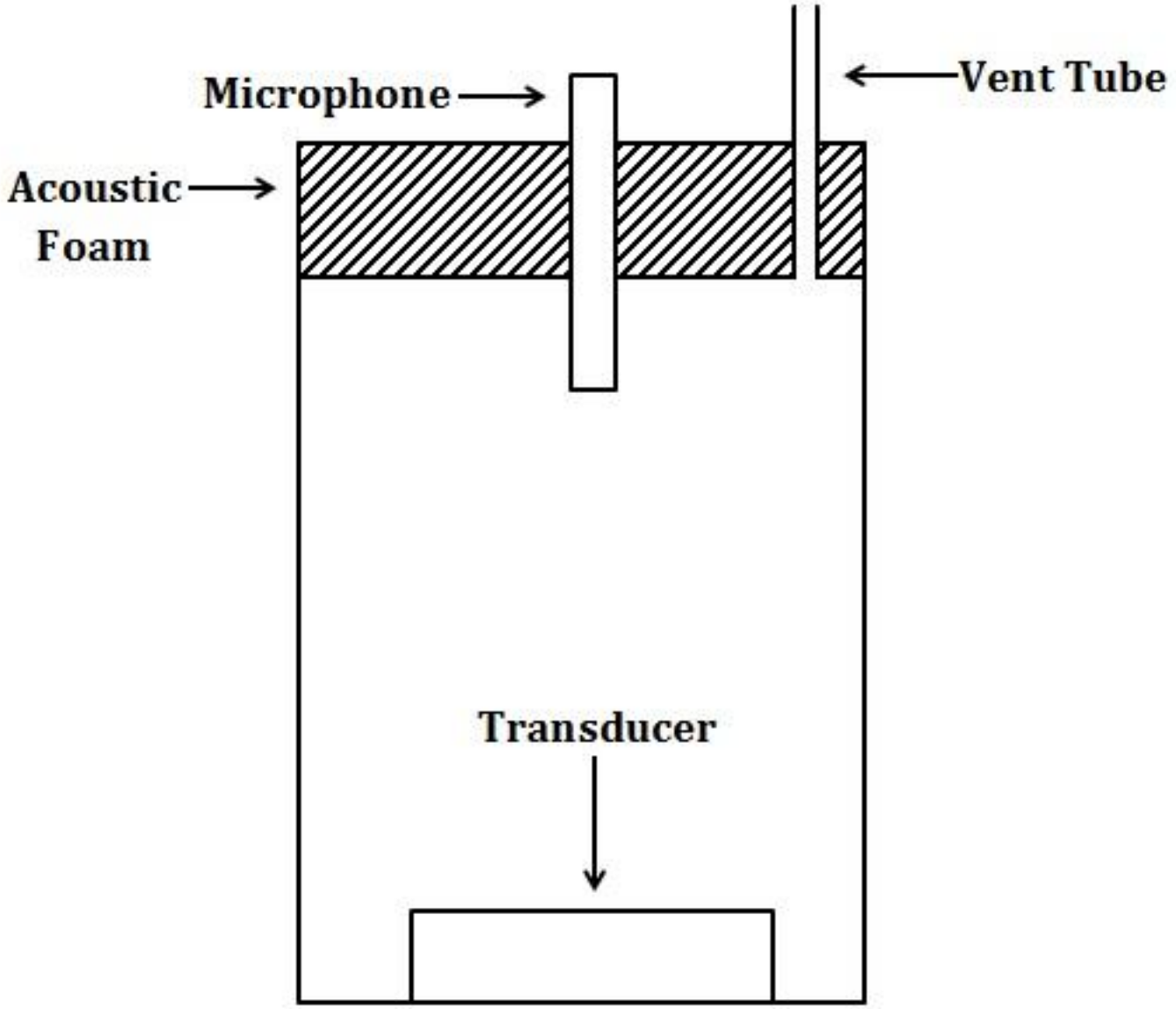

Figure 10: Plastic box for testing in rudimentary CO_2 atmosphere.

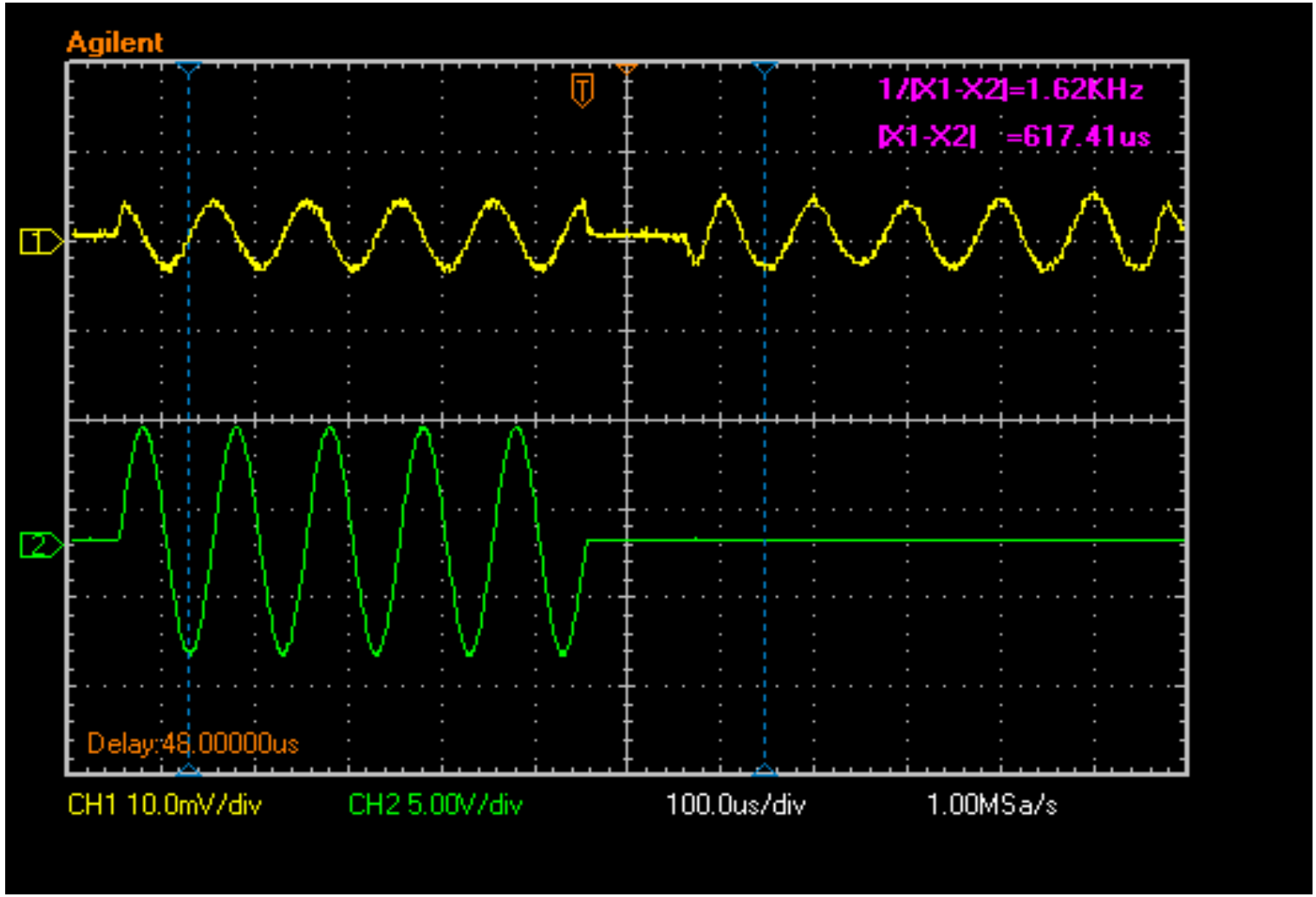

Figure 11: Oscilloscope reading for an air environment in plastic box.

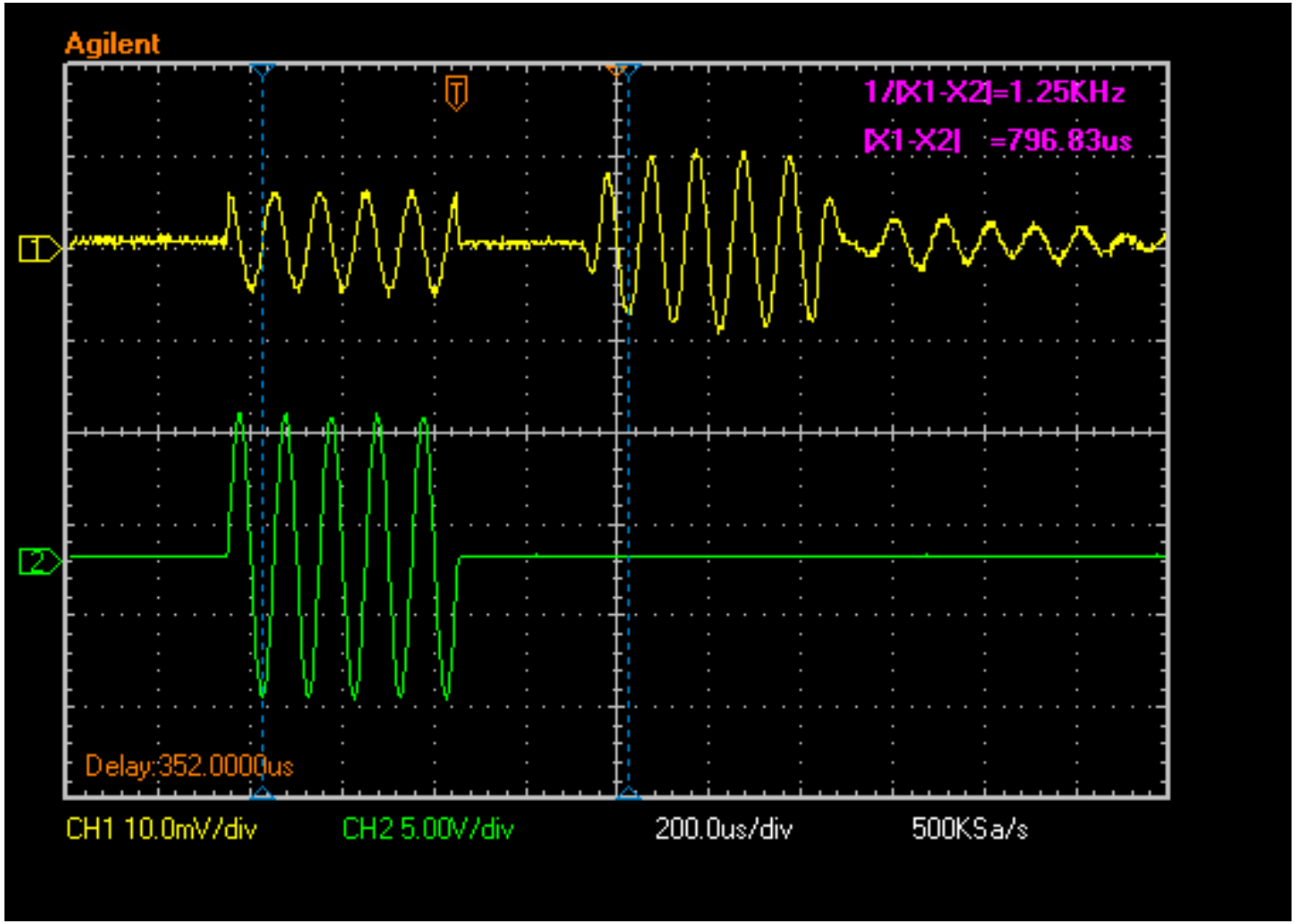

Figure 12: Oscilloscope reading for a carbon dioxide environment in plastic box.

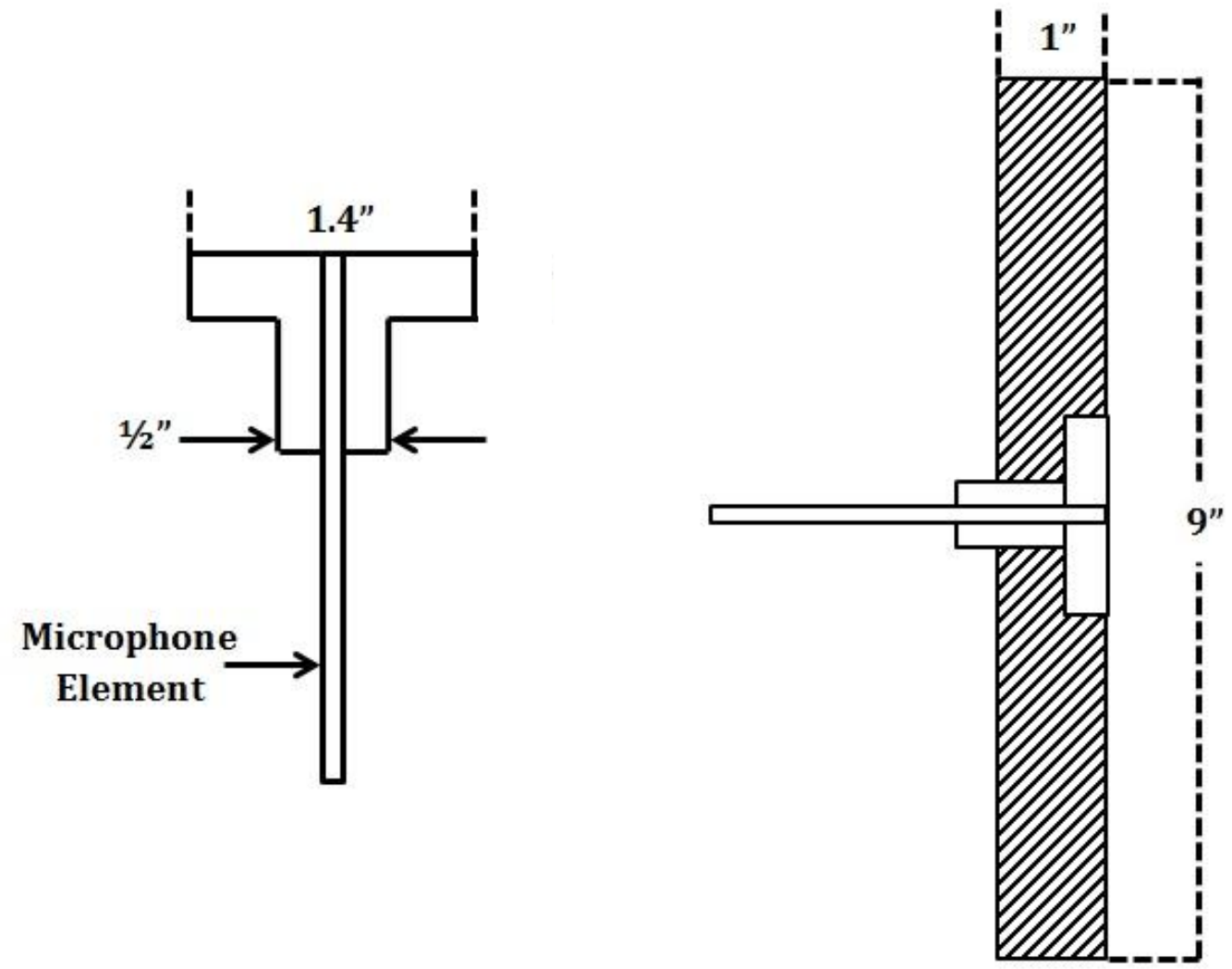

Figure 13: Microphone adapter schematic.

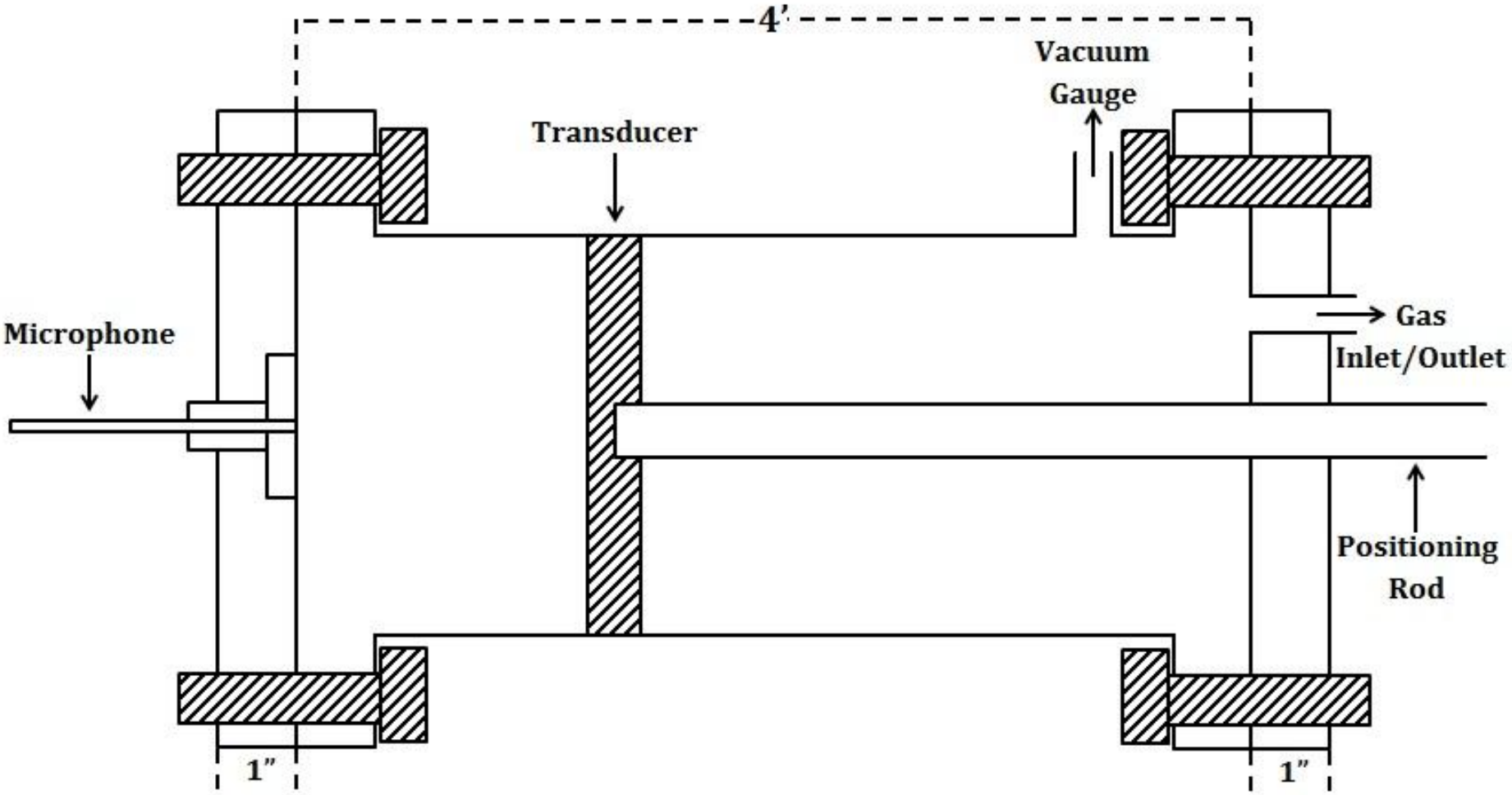

Figure 14: Setup sideways schematic.

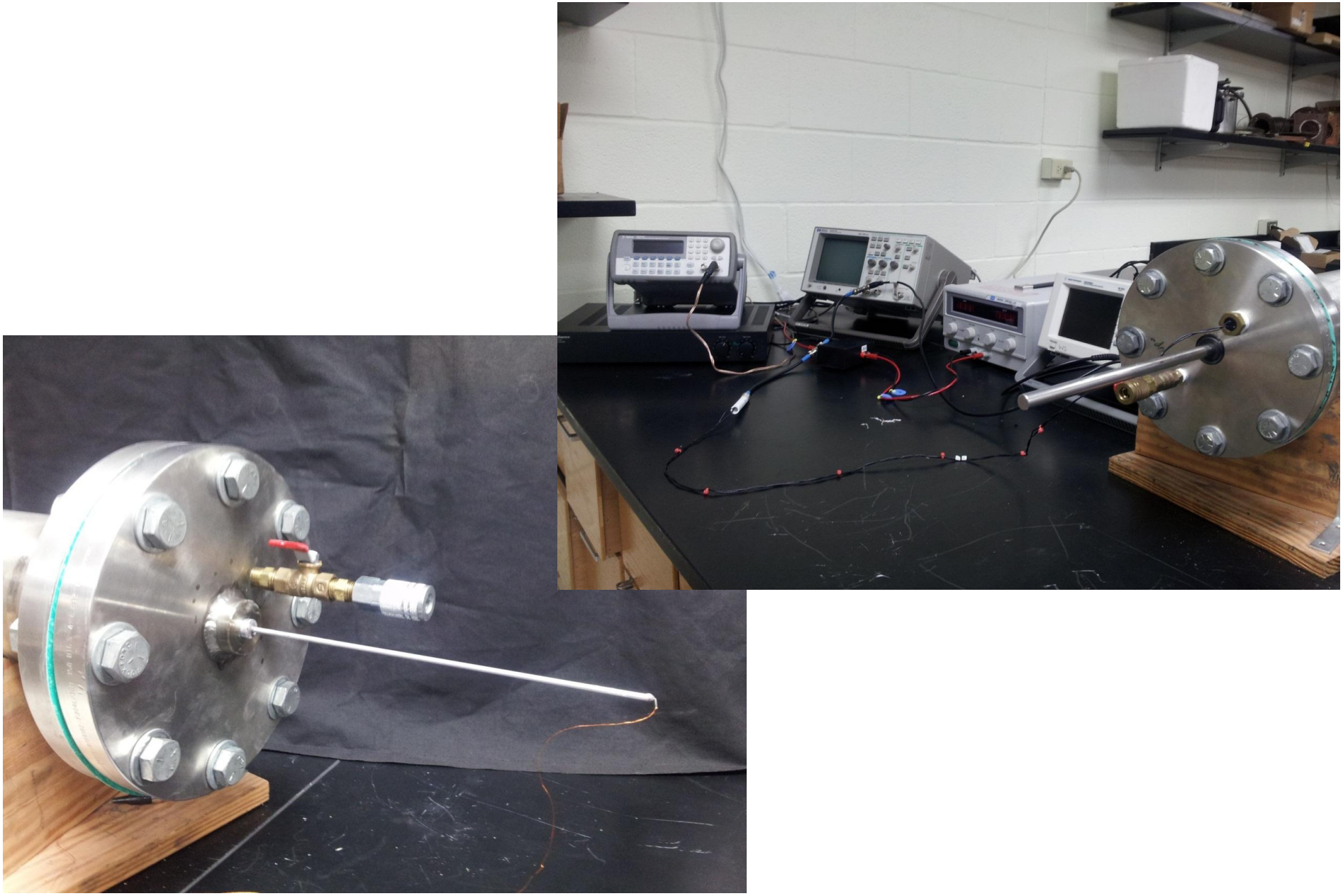

Figure 15: Actual photos of microphone flange (left) and electronic equipment with transducer positioning flange (right).

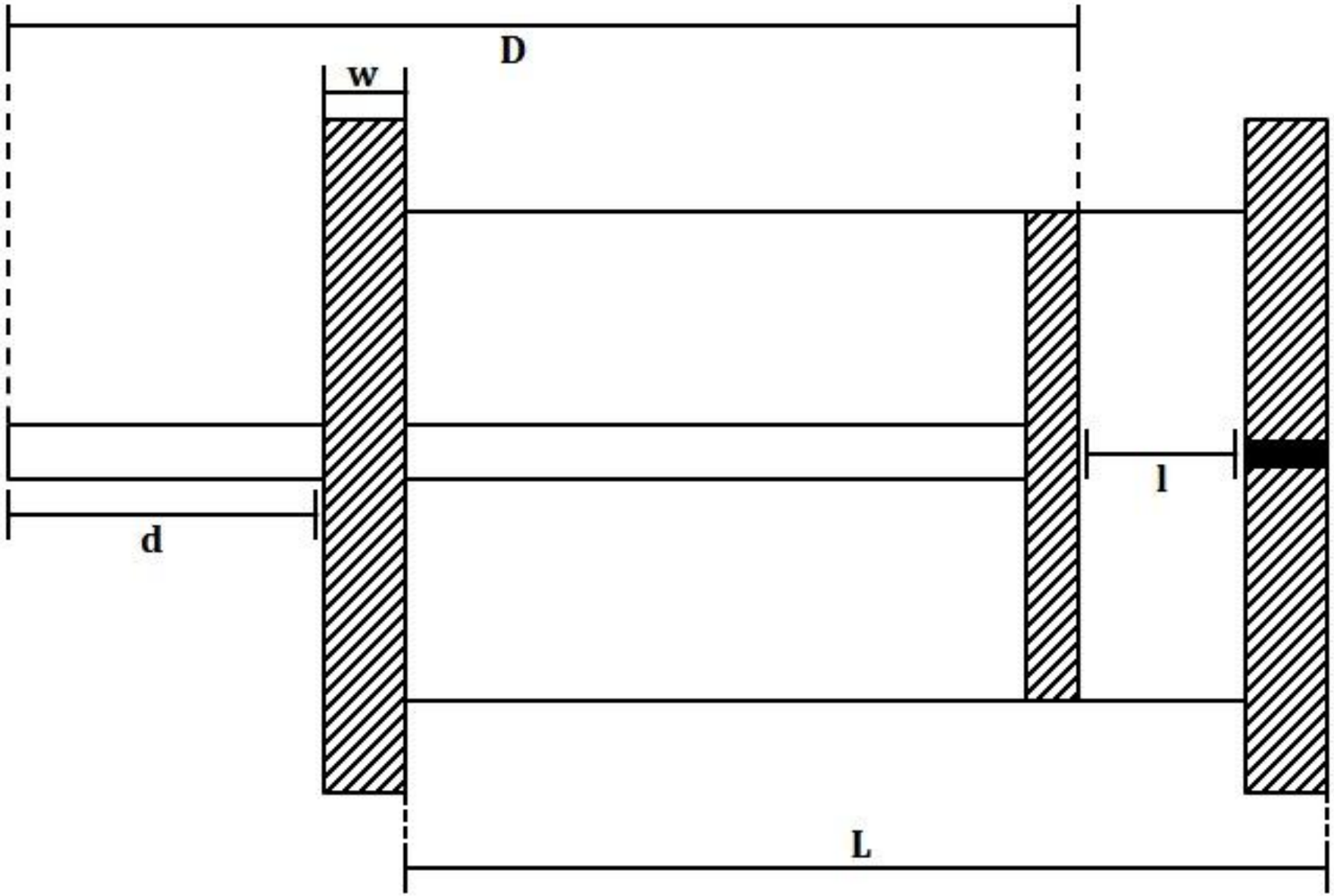

Figure 16: Schematic of how to roughly calculate length between the transducer face and microphone.

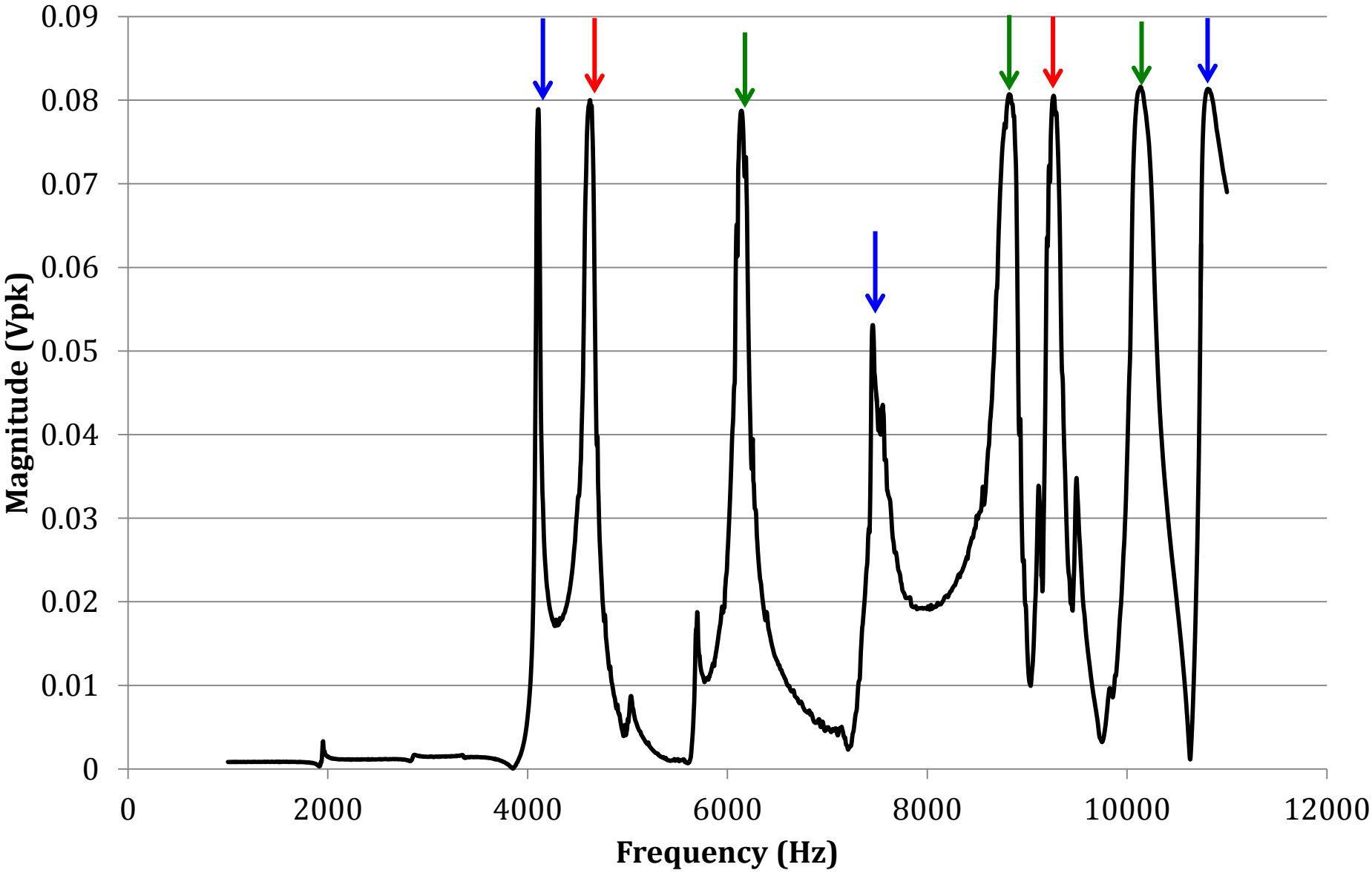

Figure 17: Frequency versus magnitude for 1-11 kHz range in air.

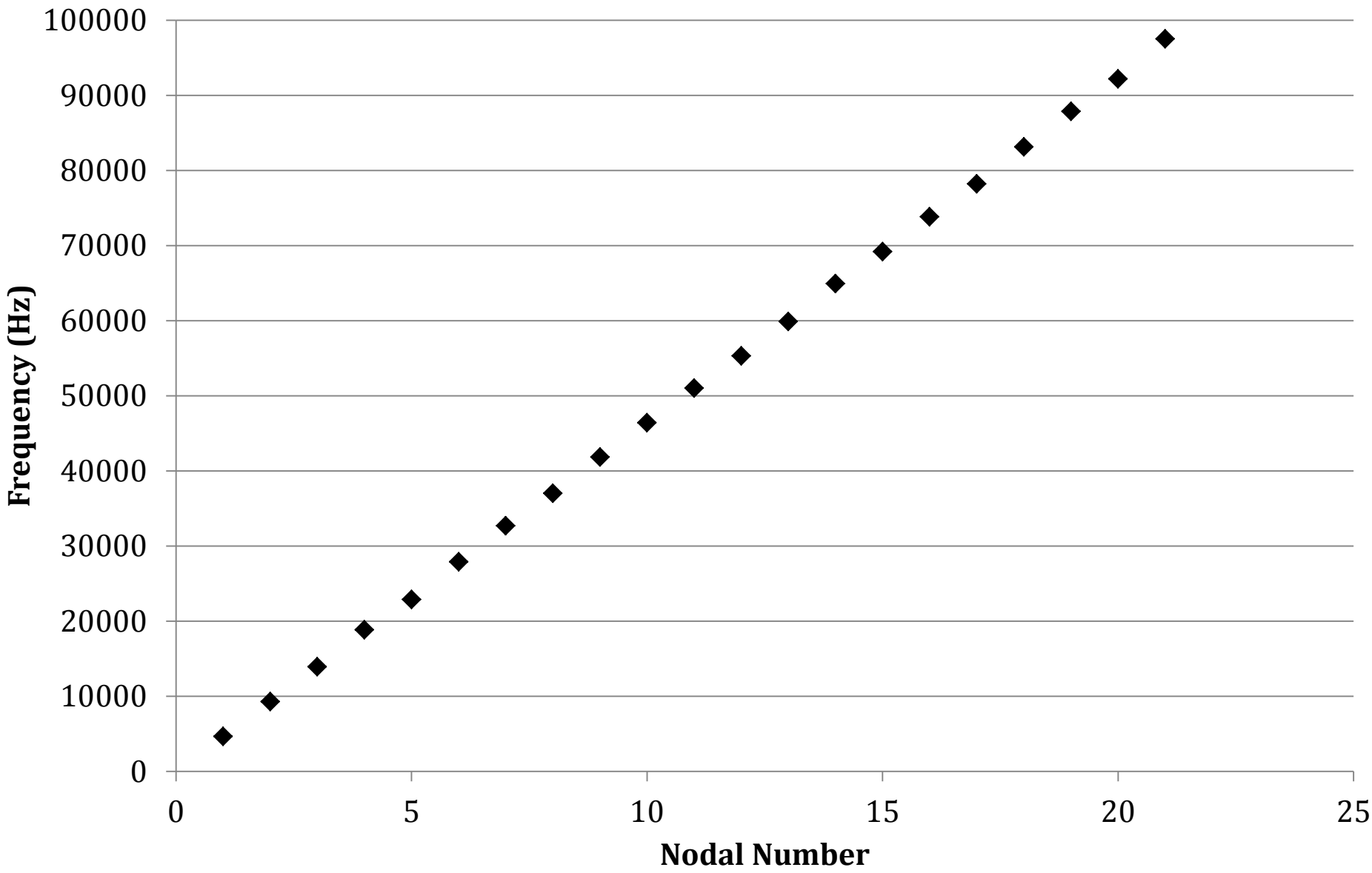

Figure 18: Frequency versus nodal number, *n*, for the entire air data set.

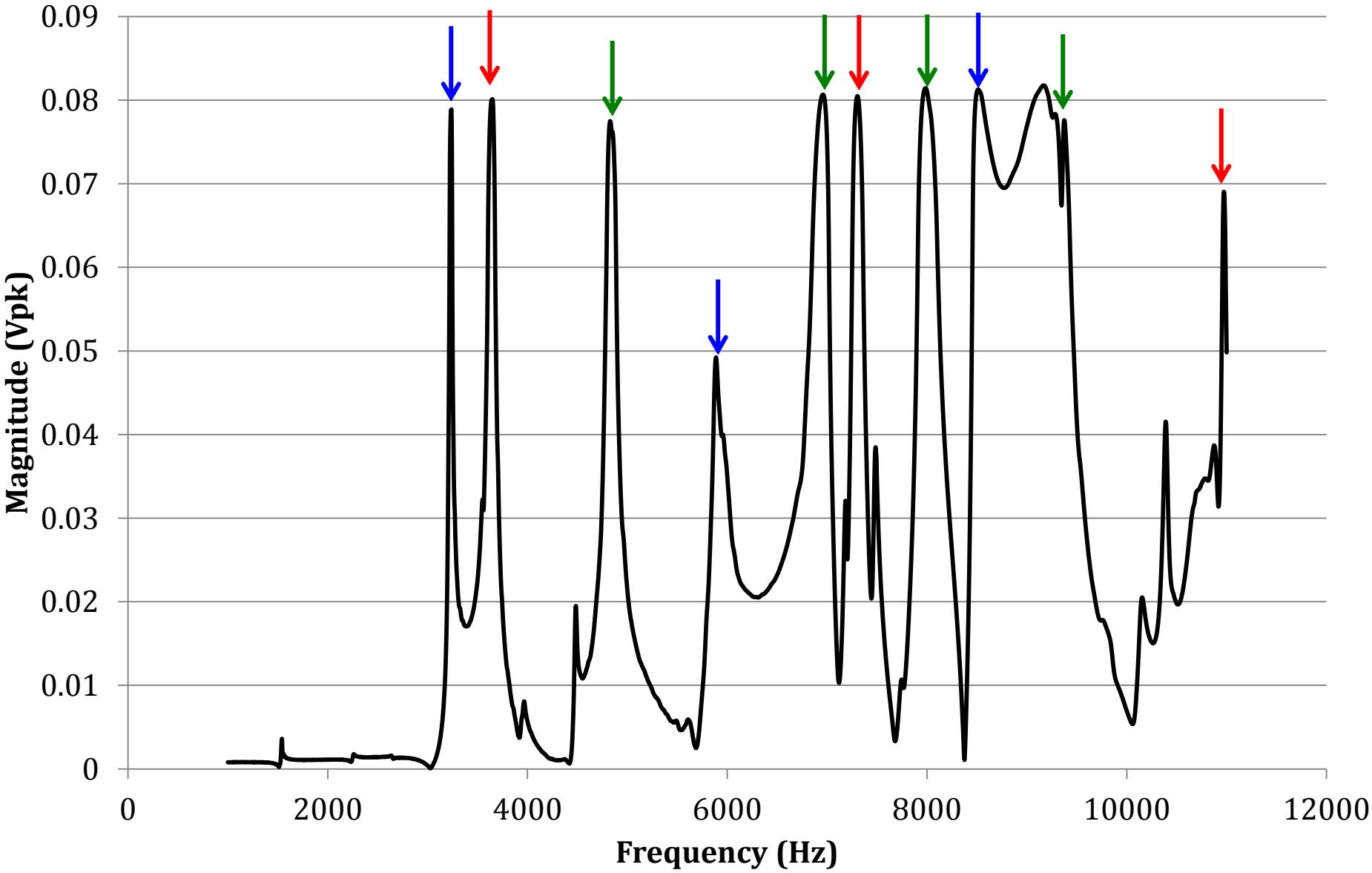

Figure 19: Frequency versus magnitude for 1-11 kHz range in CO_2.

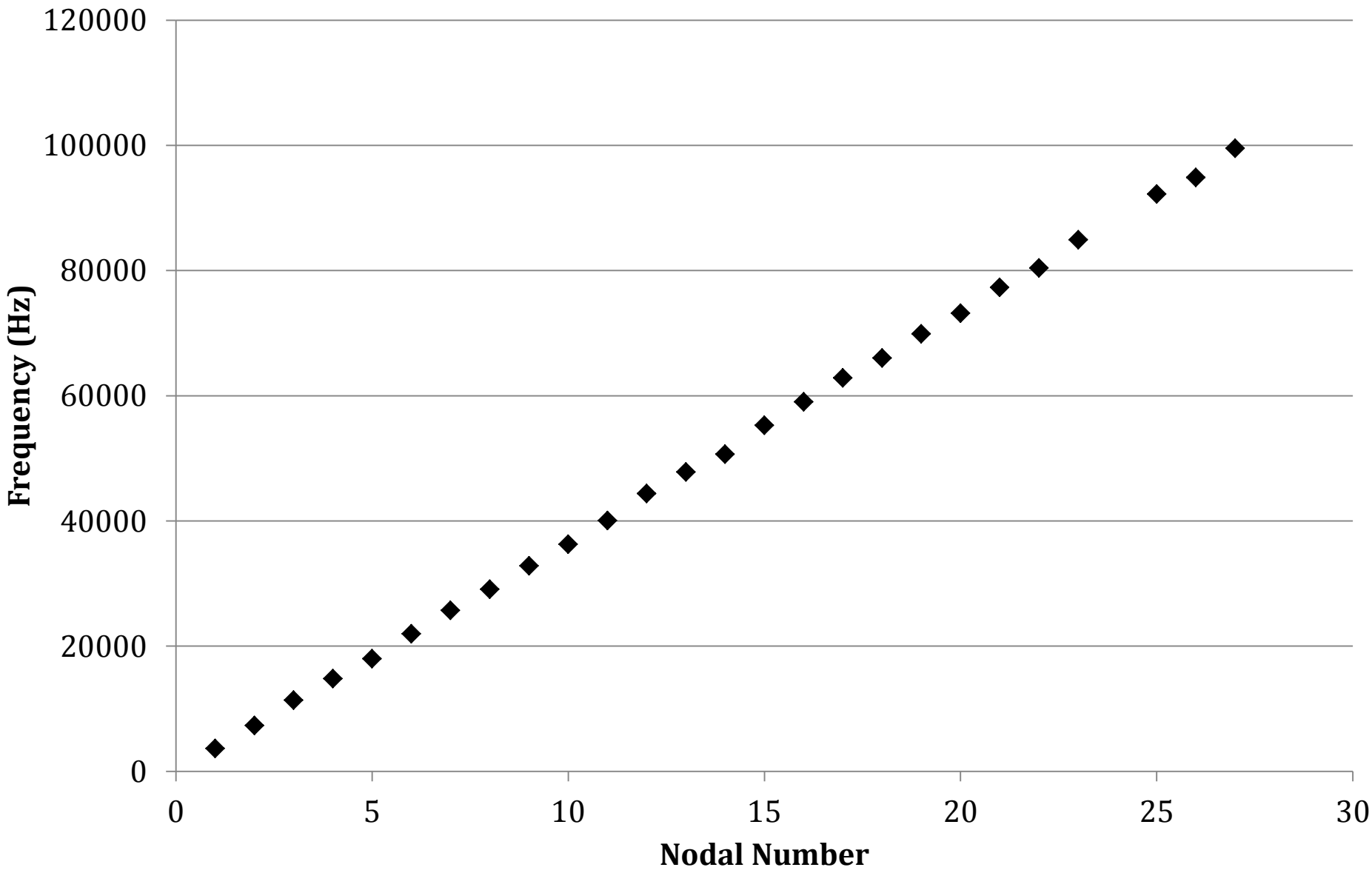

Figure 20: Frequency versus nodal number, *n*, for the entire CO_2 data set.

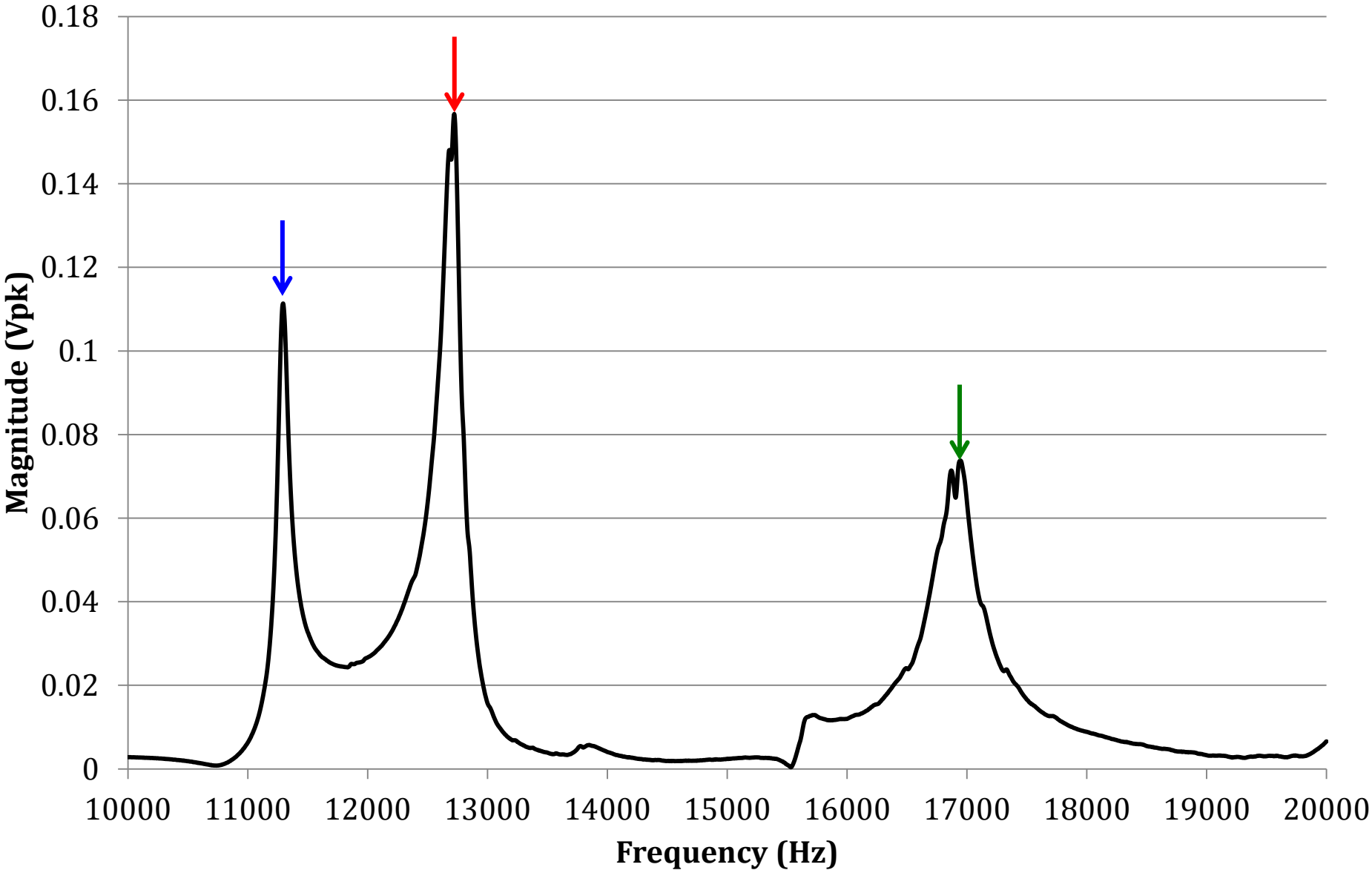

Figure 21: Frequency versus magnitude for the 10-20 kHz range in helium.

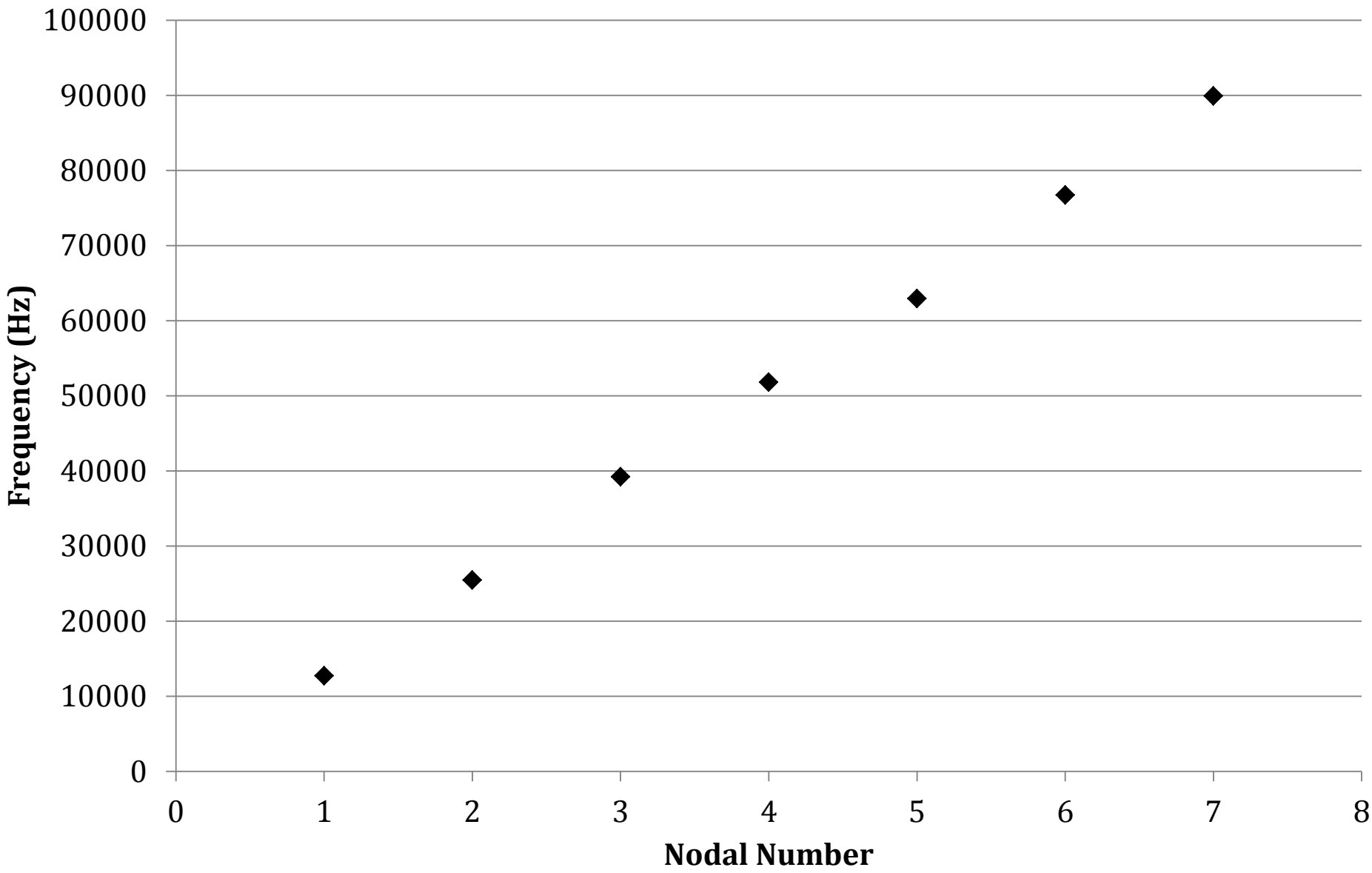

Figure 22: Frequency versus nodal number, *n*, for the entire helium data set.

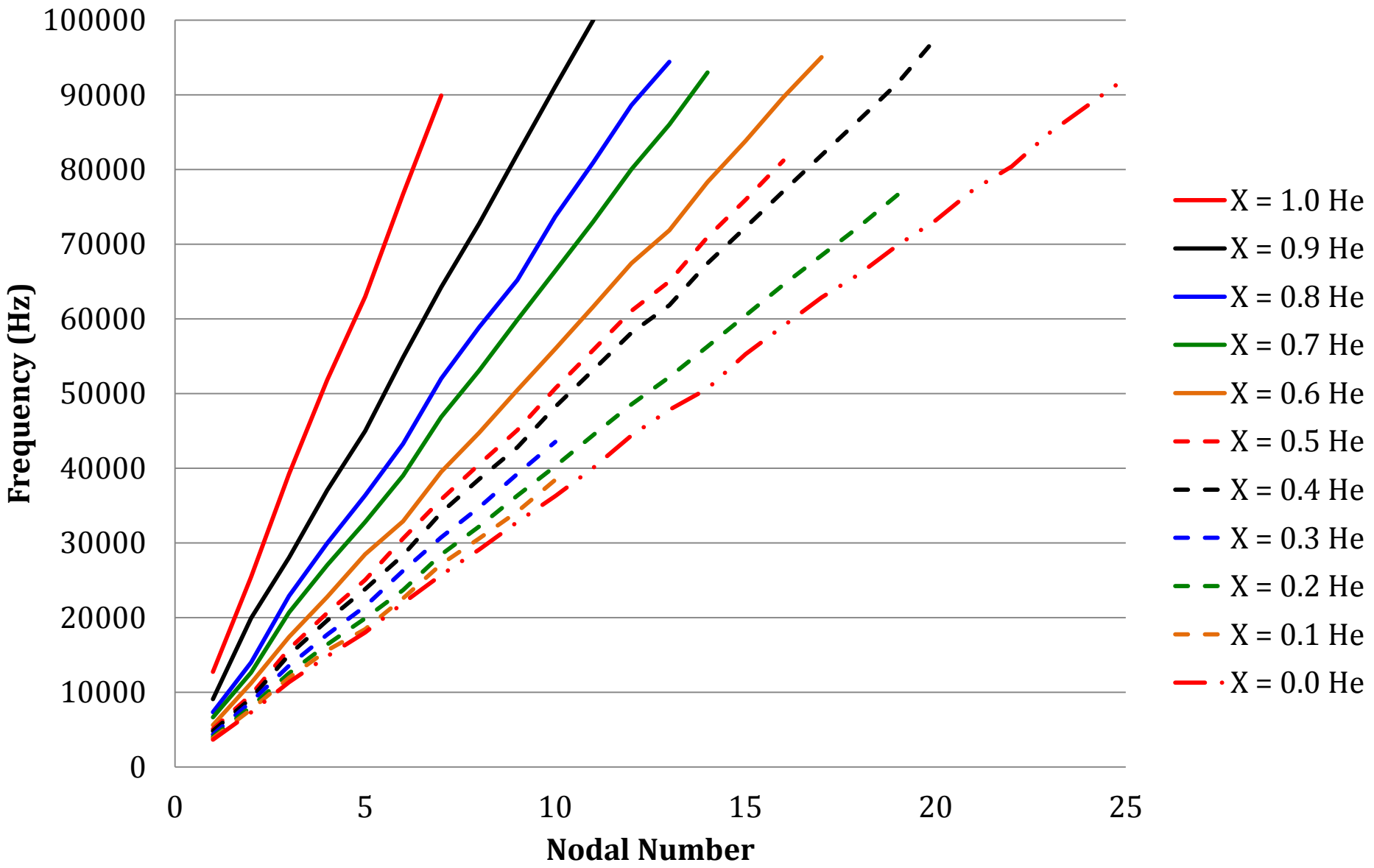

Figure 23: Frequency versus nodal number, *n*, for mixtures with partial pressure *X* of helium in CO_2.

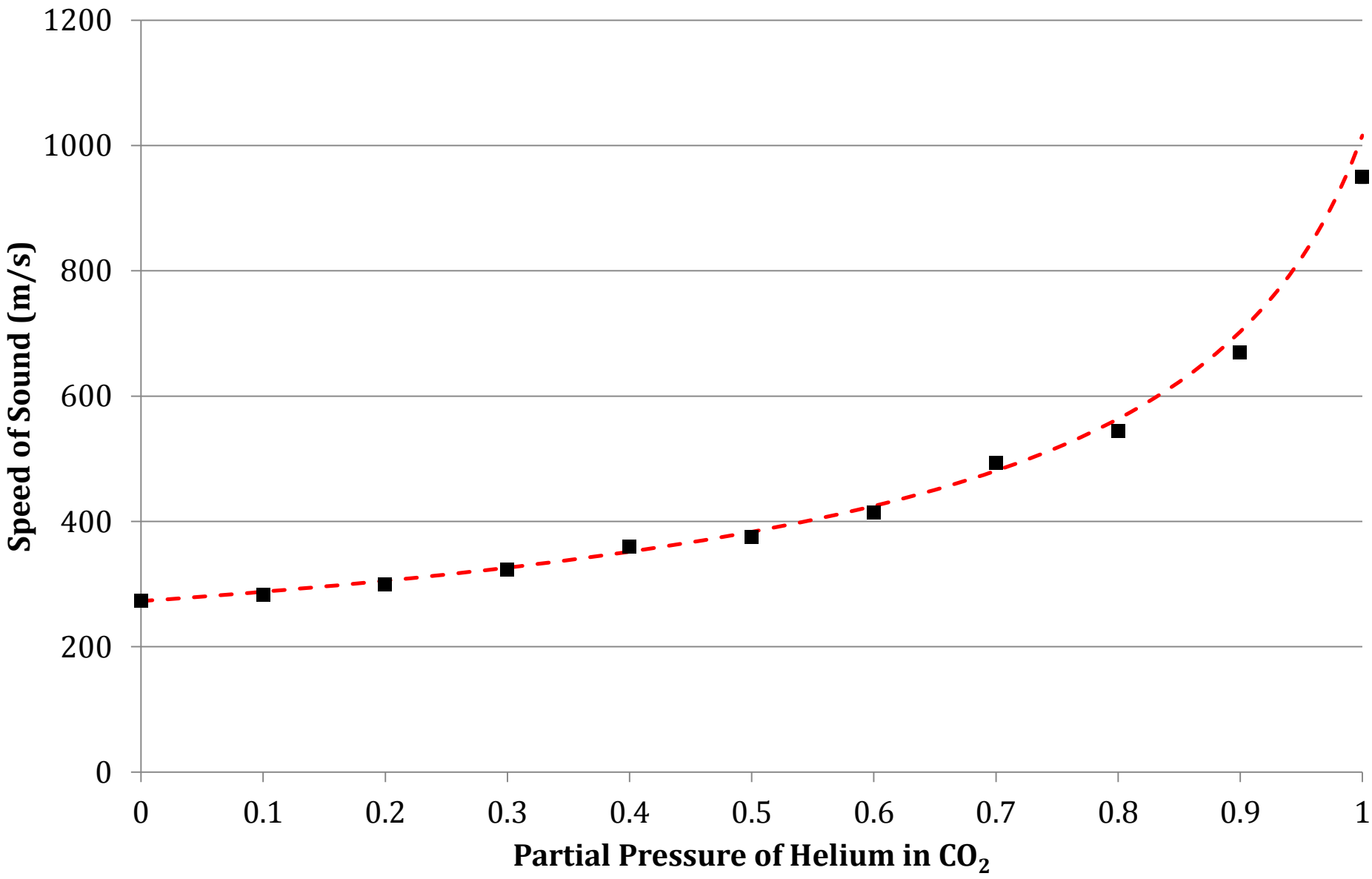

Figure 24: Theoretical values (red dashed line) and experimental values (black points) for speed of sound in helium and CO_2 mixtures.

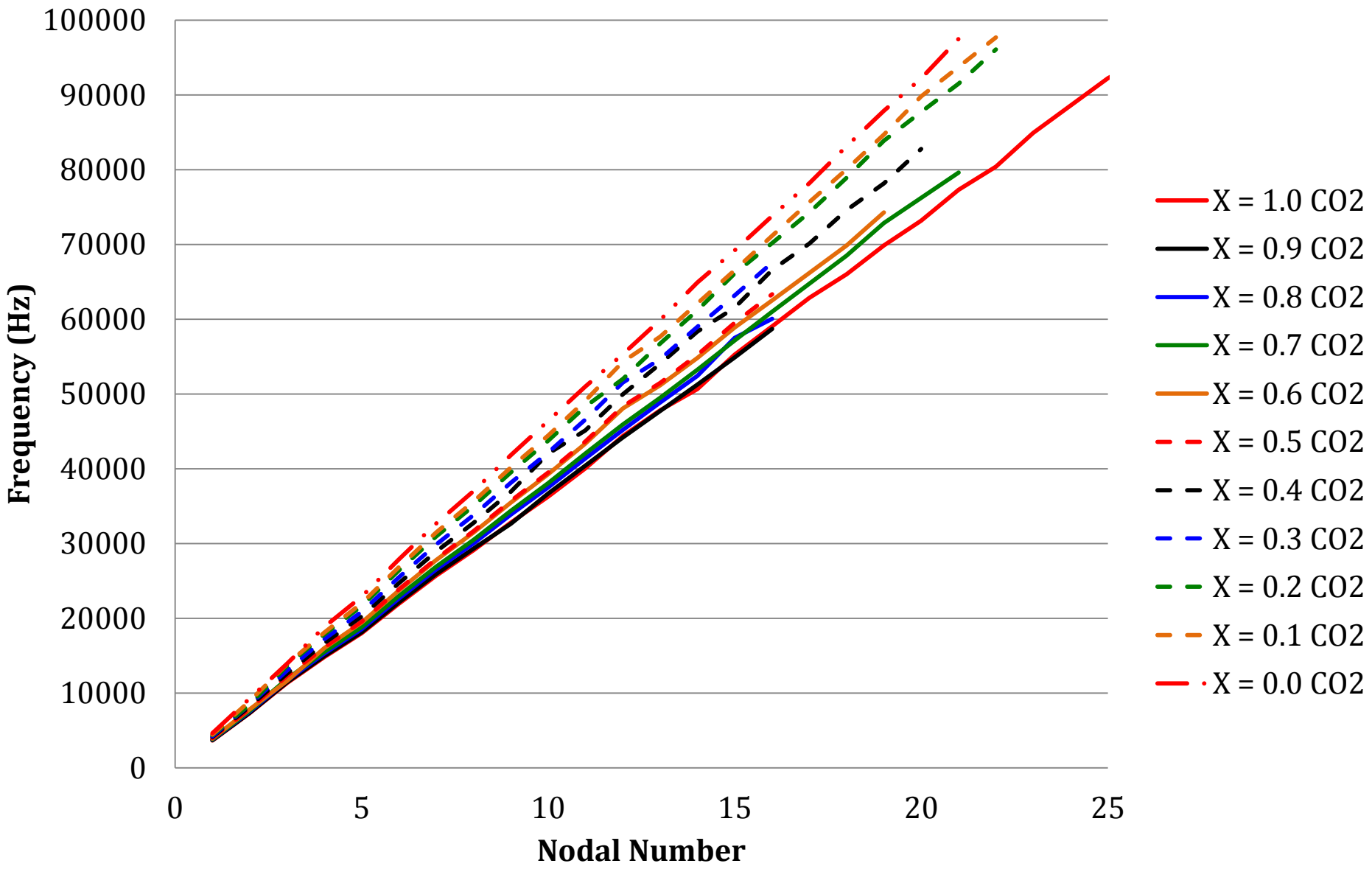

Figure 25: Frequency versus nodal number, *n*, for mixtures with partial pressure *X* of CO_2 in air.

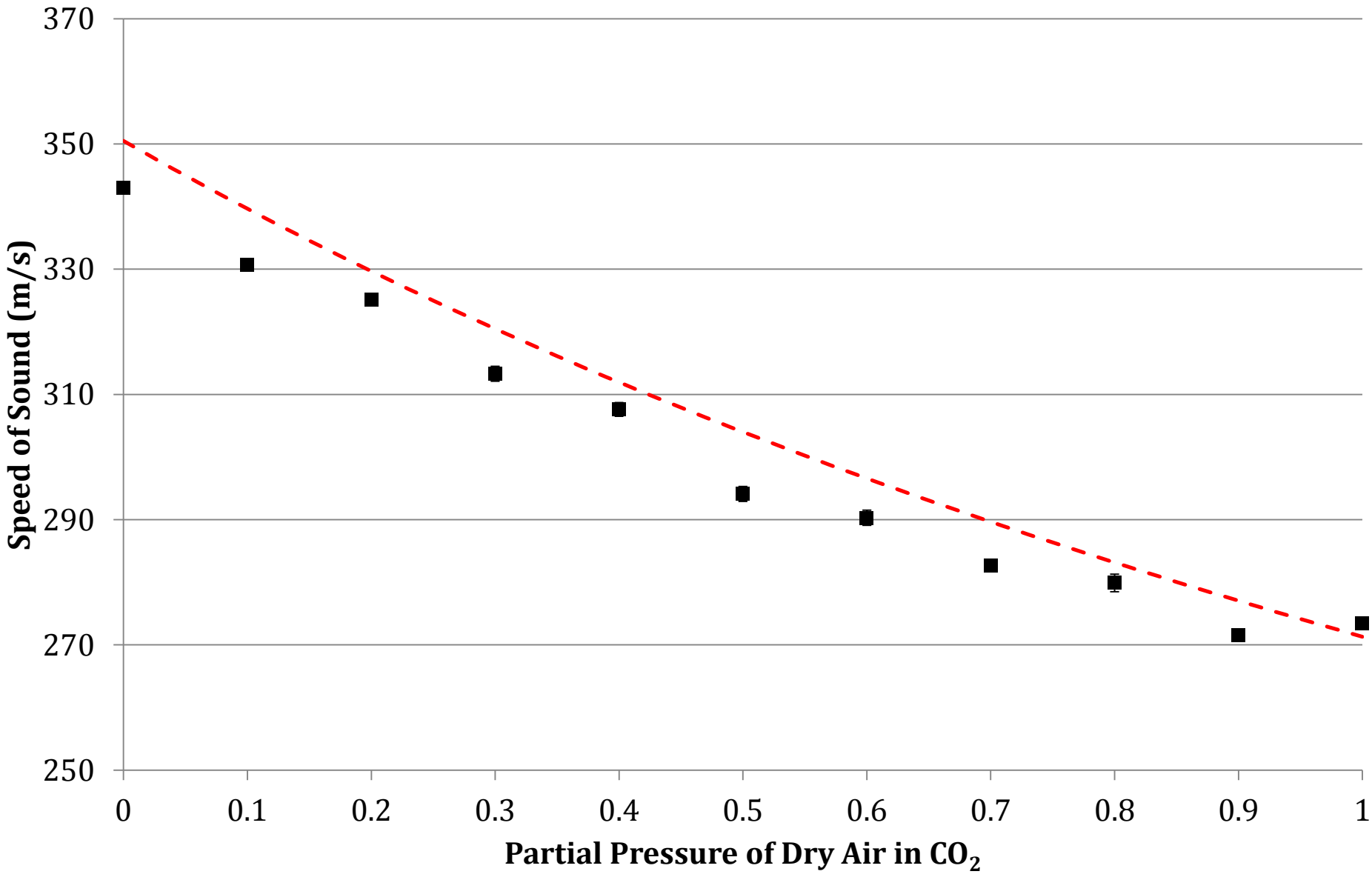

Figure 26: Theoretical values (red dashed line) and experimental data (black points) for speed of sound in CO_2 and dry air mixtures.

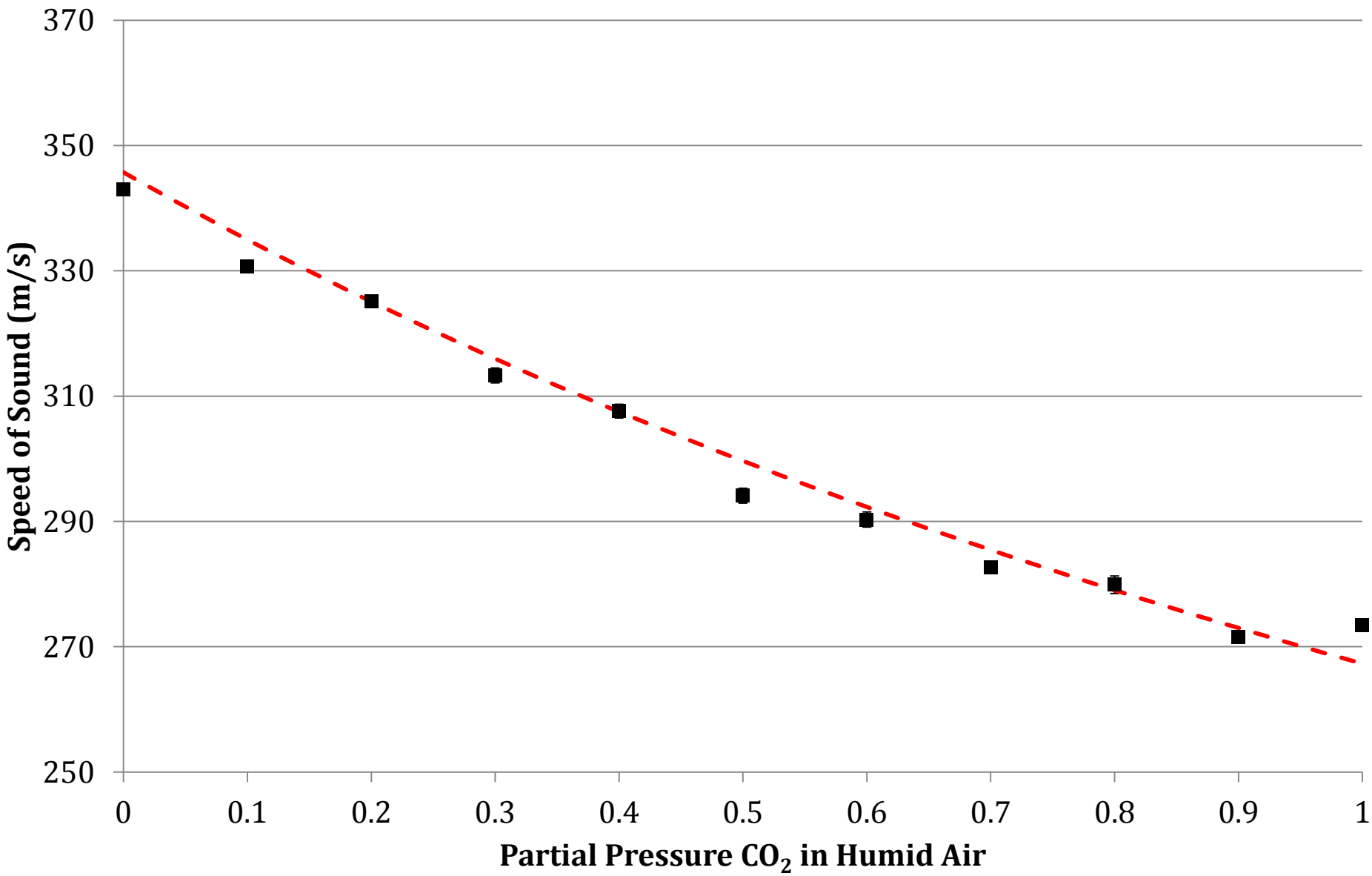

Figure 27: Theoretical values (red dashed line) and experimental data (black points) for speed of sound in CO_2 and humid air mixtures.

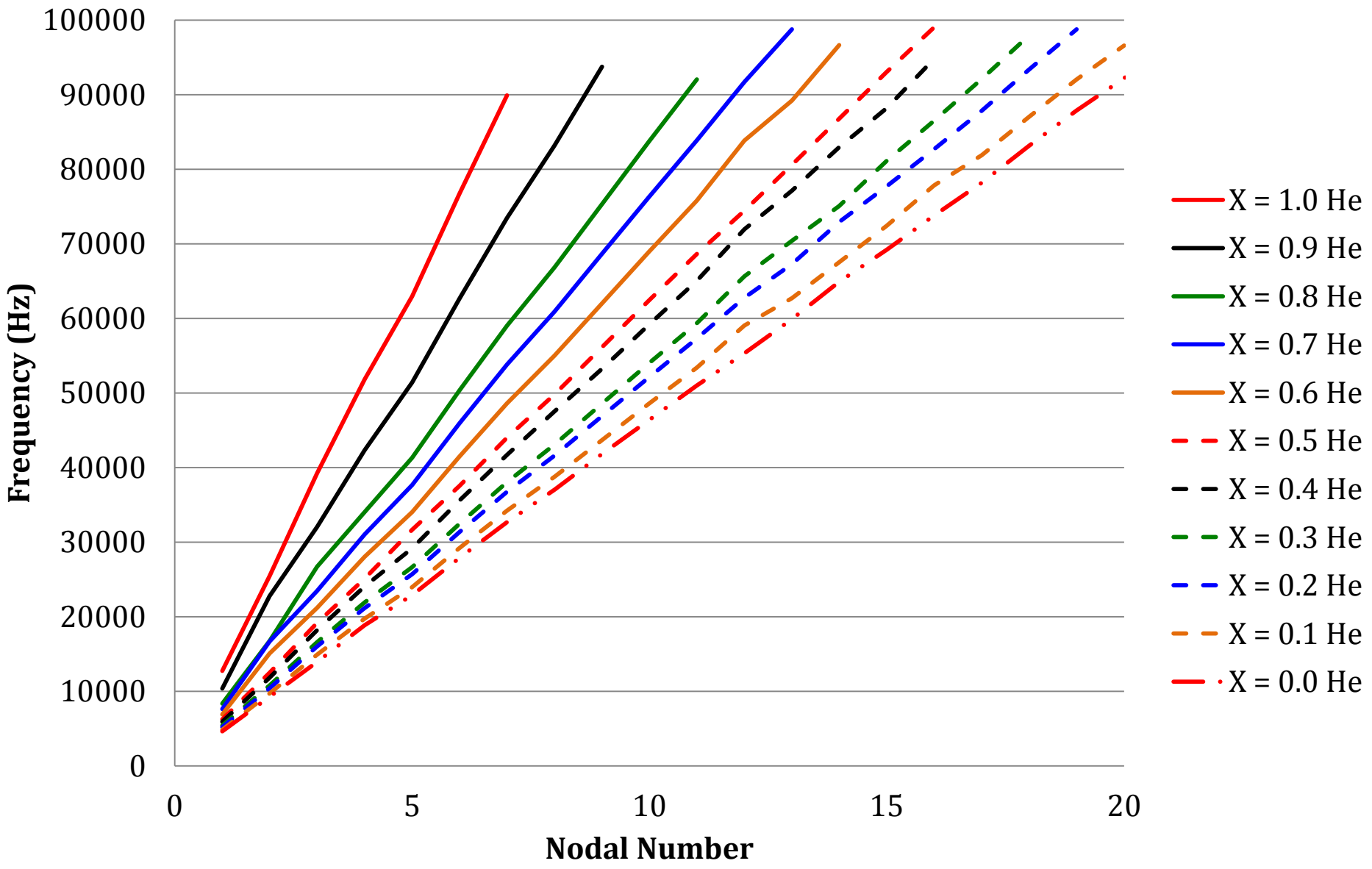

Figure 28: Frequency versus nodal number, *n*, for mixtures with partial pressure *X* of helium in air.

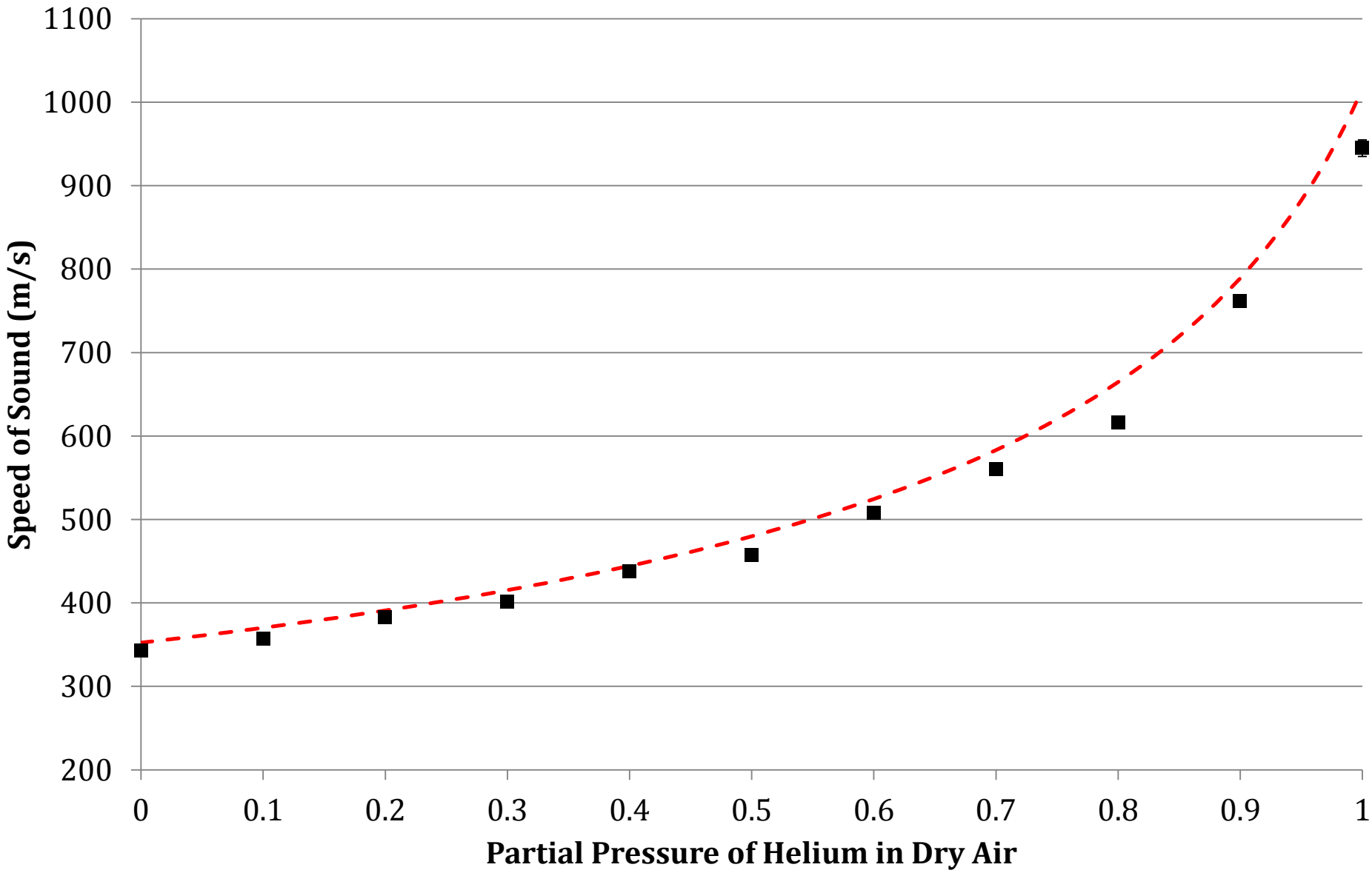

Figure 29: Theoretical values (red dashed line) and experimental data (black points) for speed of sound in helium and dry air mixtures.

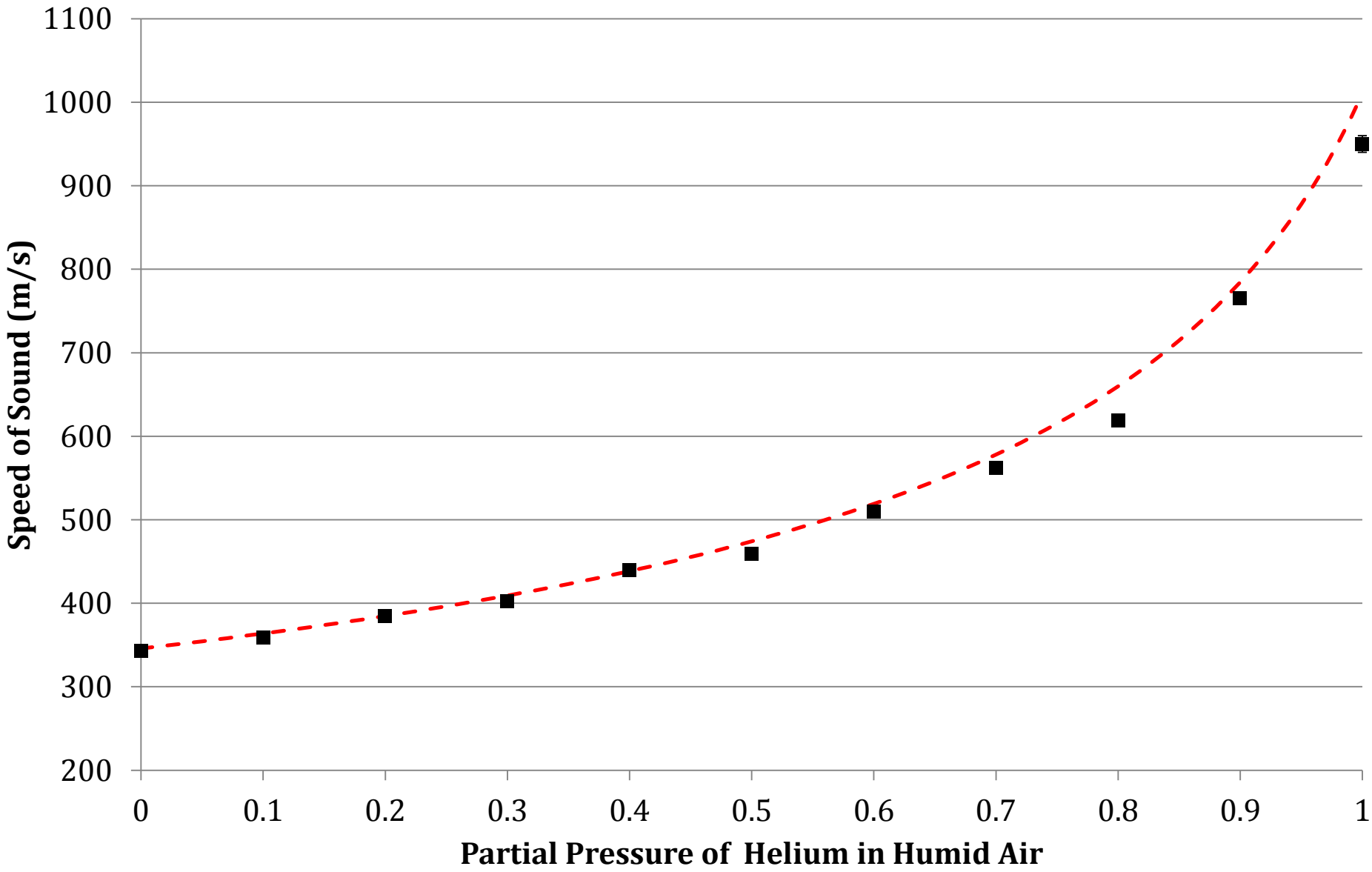

Figure 30: Theoretical values (red dashed line) and experimental data (black points) for speed of sound in helium and humid air mixtures.